JOURNAL OF THE ROYAL SOCIETY Interface

Interfacial energetics of globular–blood protein adsorption to a hydrophobic interface from aqueous-buffer solution

Anandi Krishnan, Yi-Hsiu Liu, Paul Cha, David Allara and Erwin A Vogler

J. R. Soc. Interface 2006 **3**, 283-301
doi: 10.1098/rsif.2005.0087

JOURNAL OF THE ROYAL SOCIETY Interface

J. R. Soc. Interface (2006) **3**, 283–301
doi:10.1098/rsif.2005.0087
Published online 17 October 2005

Interfacial energetics of globular–blood protein adsorption to a hydrophobic interface from aqueous-buffer solution

Anandi Krishnan[1], Yi-Hsiu Liu[2], Paul Cha[2], David Allara[2,3,4] and Erwin A. Vogler[2,3,5,*]

[1]*Department of Bioengineering,* [2]*Department of Materials Science and Engineering,* [3]*Materials Research Institute,* [4]*Department of Chemistry, and* [5]*Huck Institute of Life Sciences, The Pennsylvania State University, University Park, PA 16802, USA*

Adsorption isotherms of nine globular proteins with molecular weight (MW) spanning 10–1000 kDa confirm that interfacial energetics of protein adsorption to a hydrophobic solid/aqueous-buffer (solid–liquid, SL) interface are not fundamentally different than adsorption to the water–air (liquid–vapour, LV) interface. Adsorption dynamics dampen to a steady-state (equilibrium) within a 1 h observation time and protein adsorption appears to be reversible, following expectations of Gibbs' adsorption isotherm. Adsorption isotherms constructed from concentration-dependent advancing contact angles θ_a of buffered-protein solutions on methyl-terminated, self-assembled monolayer surfaces show that maximum advancing spreading pressure, Π_a^{max}, falls within a relatively narrow $10 < \Pi_a^{max} < 20$ mN m^{-1} band characteristic of all proteins studied, mirroring results obtained at the LV surface. Furthermore, Π_a isotherms exhibited a 'Traube-rule-like' progression in MW similar to the ordering observed at the LV surface wherein molar concentrations required to reach a specified spreading pressure Π_a decreased with increasing MW. Finally, neither Gibbs' surface excess quantities $[\Gamma_{sl}-\Gamma_{sv}]$ nor Γ_{lv} varied significantly with protein MW. The ratio $\{[\Gamma_{sl}-\Gamma_{sv}]/\Gamma_{lv}\} \sim 1$, implying both that $\Gamma_{sv} \sim 0$ and chemical activity of protein at SL and LV surfaces was identical. These results are collectively interpreted to mean that water controls protein adsorption to hydrophobic surfaces and that the mechanism of protein adsorption can be understood from this perspective for a diverse set of proteins with very different composition.

Keywords: protein adsorption; surface; solid–water interface; blood proteins; air–water interface; interphase

1. INTRODUCTION

Protein adsorption is one of the most fundamental, unsolved problems in biomaterials surface science (Vogler 1993, 1998). Practical importance of the problem is related to the fact that protein adsorption is among the first steps in the acute biological response to materials that dictates biocompatibility, and hence utility in medical-device applications. As a consequence of these scientific and pragmatic factors, the protein-adsorption problem has attracted considerable research attention from diverse fields of inquiry ranging from biomaterials to physics. An undercurrent flowing through much of this research seems to be that the amount of protein adsorbed to a surface is primarily controlled by short-range, pair-wise interactions between protein molecules and adsorbent surface (consider, for example, the RSA model of protein adsorption). Adsorbed protein is frequently assumed to be irreversibly surface bound in a monolayer arrangement (e.g. Dee *et al.* 2002 and citations therein). However, presumption of irreversible adsorption remains controversial in the literature (Vogler 1998) and multi-layering of protein has been experimentally demonstrated in a number of cases (Graham *et al.* 1979; Brynda *et al.* 1984; Jeon *et al.* 1992; Claesson *et al.* 1995; Vogler 1998; Chen *et al.* 2003; Zhou *et al.* 2004). Furthermore, the apparent specificity/selectivity of adsorption from multi-component solutions is frequently attributed to variations in protein molecular structure that give rise to differential interactions with a particular adsorbent.

It is our contention that this view of protein adsorption to surfaces does not properly account for the role of water in the process and, in so doing, fails to discern unifying trends in protein adsorption (Krishnan *et al.* 2003, 2004*a*,*b*, 2005*b*,*c*). For example, literature illustrations depict protein and adsorbent surfaces without juxtaposing hydration layers, one layer for protein and one for surface, and do not contemplate

*Author for correspondence (eav3@psu.edu).

Received 25 February 2005
Accepted 5 September 2005

how these layers are displaced or coalesced as protein and surface come into close contact. Many modern computational models probing surface–protein interactions regard water as a complicating feature that can be ignored for the sake of reasonable computational time (see Vasquez *et al.* 1994; Cramer & Truhlar 1999; Head-Gordon & Hura 2002 and citations therein). When water is included in such models, it is usually only those molecules directly adjacent to the protein that comprise the 'bound-water layer', classically measured by δ in grams-water-per-gram-protein (Durchschlag *et al.* 2001; Garcia de la Torre 2001; Harding 2001), where $\delta \sim 0.35\ \mathrm{g\,g^{-1}}$ is found to be a representative average value (Durchschlag & Zipper 2001). This protein-bound water layer falls well short of the volume which must be displaced when a protein molecule approaches a hydrated adsorbent surface. That is to say, since two objects cannot occupy the same space at the same time, a volume of interfacial water at least equal to the partial specific volume v^{o} ($0.70 \leq v^{o} \leq 0.75\ \mathrm{cm^3\,g^{-1}}$ protein) of the adsorbing protein must move (Chalikian & Breslauer 1996). If protein adsorbs in multi-layers, then clearly much more water must be displaced. Some or all of this interfacial water is bound to the adsorbent surface to an extent that varies with surface energy (Vogler 1998, 2001). Consequently, protein adsorption is found to scale with water wettability (Vogler 1992*a*,*b*; Vogler *et al.* 1993), underscoring need to incorporate surface hydration explicitly into protein–adsorption models. Indeed, accounting for water in protein adsorption has become a significant preoccupation of quartz crystal microbalance (QCM) practitioners because QCM not only measures adsorbed protein mass but also 'trapped' (Hook & Kasemo 2001) or 'intra-layer' (Hook *et al.* 1998) or 'hydrodynamically coupled' (Hook *et al.* 2002) water.

We have made use of a simplified 'core-shell' model of globular proteins in which spheroidal molecules are represented as a packed core surrounded by a hydration shell. The core has a radius r_{v} that scales with molecular weight ($\mathrm{MW}^{1/3}$) and the hydration shell has a thickness such that the ensemble radius $R = \chi r_{\mathrm{v}}$ equals the hydrodynamic radius (Krishnan *et al.* 2003), where χ is taken to be a generic factor for all proteins. Calibration to human serum albumin (FV HSA) dimensions reveals that $R = 1.3 r_{\mathrm{v}}$ (30% larger than r_{v}) and contains about 0.9 g water $\mathrm{g^{-1}}$ protein. Hence, the hydration layer accommodated by this model is *ca* 3× greater than δ. Calibrated to neutron-reflectivity (NR) of albumin adsorption to surfaces, this model suggests that protein saturates the hydrophobic surface region by packing to nearly face-centred-cubic (FCC) concentrations wherein hydration shells touch but do not overlap (Krishnan *et al.* 2003). We propose that osmotic repulsion among hydrated protein molecules limits interphase capacity. Stated another way, protein adsorption is limited by the extent to which the hydrophobic interface can be dehydrated through displacement of interfacial water by adsorbing protein. Accordingly, protein adsorption is viewed as being more about solvent than protein itself; a perspective in sharp contrast to the prevailing paradigm mentioned above.

This water-oriented perspective on protein adsorption presents a considerable simplification of the protein–adsorption process and, as a result, a tractable quasi-thermodynamic theory can be sketched out for a phenomenon that would otherwise be overwhelmingly complex for more than just a few proteins in solution. We find that this theory naturally explains the experimentally observed 'Traube-rule progression' in which molar concentrations required to fill the liquid–vapour (LV) surface follow a homology in protein size, consistent with packing hydrated spheroidal molecules within this space (Krishnan *et al.* 2003). A relatively straightforward set of 'mixing rules' follow directly, stipulating both concentration and weight-fraction distribution of proteins adsorbed to the LV surface from multi-component aqueous solutions such as blood plasma or serum (Krishnan *et al.* 2004*a*). These mixing rules rationalize the long-known-but-otherwise-unexplained observations that: (i) LV interfacial tension γ_{lv} of blood plasma and serum is nearly identical, in spite of the fact that serum is substantially depleted of coagulation proteins such as fibrinogen; and (ii) γ_{lv} of plasma and serum derived from human, bovine, ovine, and equine blood is practically identical, even though there are substantial differences in plasma proteome among these species (Krishnan *et al.* 2005).

This paper discloses results of an investigation of globular–blood protein adsorption to a well-defined, hydrophobic solid/aqueous-buffer (solid–liquid, SL) interface. Methyl-terminated, self-assembled thiol monolayers (SAMs) on gold-coated semi-conductor-grade silicon wafers exhibiting water contact angles $\theta_{\mathrm{a}} \sim 110°$ are used as test substrata. Time-and-concentration-dependent contact angles measure adsorption energetics of (globular) proteins spanning three decades in MW in a manner parallel to the above-cited studies of protein adsorption to the LV surface. We find that the basic pattern observed at the LV surface is repeated at the hydrophobic SL surface, supporting our contention that water is the significant controller of protein adsorption to surfaces.

2. MATERIAL AND METHODS

2.1. Purified proteins and synthetic surfactants

Table 2 compiles pertinent details on proteins and surfactants used in this work. Protein purity was certified by the vendor to be no less than the respective values listed in column 4 of table 2, as ascertained by electrophoresis (SDS-PAGE or IEP). Mass, concentration, and molecular weights supplied with purified proteins were accepted without further confirmation. Issues associated with protein purity, especially contamination with surfactants, and the potential effect on measured interfacial tensions have been discussed elsewhere (Krishnan *et al.* 2004*b*). The single value given in table 2 (column 5) for physiological concentration of human proteins applied in this work was middle of the range listed by Putnam (Putnam 1975). Serial dilutions of protein stock solutions (usually

10 mg ml^{-1}) were performed in 96-well microtiter plates by (typically) 50 : 50 dilution in phosphate buffered saline solution (PBS; 0.14 M NaCl, 0.003 M KCl) prepared from powder (Sigma Aldrich) in distilled–deionized (18.2 MΩ cm^{-1}) water using procedures detailed in Krishnan *et al.* (2004*b*). Between 24 and 30 dilutions were prepared in this manner, covering a dynamic range between 10^{-10} and 1% (w/v), taking care to mix each dilution by repeated pipette aspiration and avoiding foaming of concentrated solutions.

2.2. Surfaces

Methyl-terminated, self-assembled monolayer surfaces (SAMs) were prepared according to standard methods of surface engineering (Nuzzo & Allara 1983; Allara & Nuzzo 1985; Nuzzo *et al.* 1987, 1990; Porter *et al.* 1987). Briefly, silicon wafers were pre-cleaned in hot 1 : 4 H_2O_2 (30%)/H_2SO_4 followed by rinsing with distilled–deionized H_2O and absolute ethanol. Gold-coated wafers were prepared by vapour deposition of chromium and gold (99.99% purity) from resistively heated tungsten boats onto clean 3 in. diameter silicon wafers at about 1×10^{-8} torr base pressure in a cryogenically pumped deposition chamber. The sample was not allowed to rise above *ca* 40 °C during the evaporation. Film thicknesses, monitored with a quartz crystal oscillator, were typically 15 and 200 nm for chromium and gold, respectively. Chromium was deposited prior to gold to enhance adhesion to the substrate. After deposition, the chamber was backfilled with research-grade nitrogen. Gold-coated samples were removed and immersed in 1 mM solutions of 1-hexadecanethiol ($CH_3(CH_2)_{15}SH$) in ethanol, contained in glass jars at ambient temperature, for at least 3 days.

The alkanethiol (Aldrich Chemical Co., Milwaukee, WI) and ethanol (commercial reagent-grade) were used as-received, without further purification. Samples were stored in the thiol solution until use and were rinsed with ethanol just prior to an experiment.

2.3. Tensiometry and goniometry

Liquid–vapour interfacial tensions required by this work were measured by Pendant Drop Tensiometry (PDT) as described in Krishnan *et al.* (2003, 2004*b*). Tilting-Plate Goniometry (TPG) was performed using a commercial-automated goniometer (First Ten Angstroms, Inc., Portsmouth, VA). Advancing contact angles (θ_a) applied in this work have been verified to be in statistical agreement with those obtained by Wilhelmy Balance Tensiometry (WBT) and Captive-Drop Goniometry as detailed in Krishnan *et al.* (2005*b*). Receding angles (θ_r) were shown to be not as reliable as θ_a and, as a consequence, only θ_a was analysed in this work. The TPG employed a Tecan liquid-handling robot to aspirate 12 µl of solutions contained in a 96-well microtiter plate prepared by the serial-dilution protocol mentioned above. The robot was used to reproducibly transfer the tip with fluid contents into a humidified (99+% RH) analysis chamber and dispense 10 µl drops of protein solution onto the surface of test substrata (see below) held within the focal plane of a magnifying camera. These and all other aspects of TPG were performed under computer control. Proprietary algorithms supplied by the vendor were used to deduce contact angles from drop images captured at a programmed rate by a frame grabber. Typically, 600 images were captured at a rate of one image every 6 s following 20 s delay to permit vibrations of the expelled drop to dampen. Drop evaporation rates within the humidified chamber deduced from computed-drop volumes (based on image analysis) were observed to vary with solute concentration, generally ranging from approximately 25 nl min^{-1} for pure water to 10 nl min^{-1} for solute solutions greater than 0.1 w/v%. The impact of this evaporation rate over the 60 min time frame of the experiment was apparently negligible, as gauged from the behaviour of purified surfactants discussed in §4. Precision of θ_a was about 0.5° based on repeated measurement of the same drop. The analysis chamber was thermostated to a lower-limit of 25±1 °C by means of a computer-controlled resistive heater. Upper-temperature limit was not controlled but rather floated with laboratory temperature, which occasionally drifted as high as 29 °C during summer months. Thus, reported θ_a values were probably not more accurate than about 1° on an inter-sample basis considering the small, but measurable, variation of water interfacial tension with temperature. This range of accuracy was deemed adequate to the conclusions of this report which do not strongly depend on more highly accurate θ_a that is difficult to achieve on a routine basis. Instead, veracity of arguments raised herein depend more on a breadth of reliable measurements made across the general family of human proteins.

Test substrata were held on a rotating, tilting-plate platform driven by stepper motors under computer control. Substrata were allowed to come to equilibrium within the sample-chamber environment for no less than 30 min before contact angle measurements were initiated. The platform was programmed to tilt at 1° s^{-1} from horizontal to 25° after the drop was deposited on the surface by the robot. The optimal (incipient rolling) tilt angle was found to be 25 and 15° for solutions of proteins and surfactants, respectively. The first 20 images monitored evolution of the advancing angle. At the end of the 1 h θ_a measurement period, the platform was programmed to return to horizontal and rotate 15° to the next analysis position along the periphery of the semi-conductor wafer. This process was repeated for all dilutions of the protein under study so that results reported for each protein were obtained on a single test surface, eliminating the possibility of substratum-to-substratum variation within reported results.

θ_a measurements by TPG employed in this work were verified against WBT and found to agree within a percentage difference of 2.5±1.9% for $50°<\theta_a<120°$ (Krishnan *et al.* 2005*b*). It is worthwhile mentioning in this context that WBT itself is inappropriate for studies of protein adsorption at the SL interface (at least as applied herein) because: (i) the technique requires thin plates that are difficult to two-side coat with gold for

thiol-SAM preparation, (ii) WBT, generally, requires high solution volumes (*ca* 10 ml) that greatly exceed availability of purified proteins, and (iii) the moving three-phase line deposits solute (protein or surfactant) at the SV interface making interpretation of the Gibbs' surface excess parameter $[\Gamma_{sl}-\Gamma_{sv}]$ highly ambiguous (Vogler 1993). Overall, we have found the tilting-plate method applicable to measuring adsorption, at least for hydrophobic surfaces, and suitable for 1 h equilibration times if a humidified chamber is used to control evaporation (Vogler 1992*a*,*b*). However, it was observed that SAM surfaces were slightly unstable and subject to 'hydration' that led to a systematic decrease in water/PBS contact angles with time. These hydration dynamics were observed to be more pronounced on SAM surfaces that had been incubated for long periods (greater than 3 d) in the 100% RH atmosphere of the PDT analysis chamber (not shown). However, we do not believe this slight but apparently unavoidable attribute of SAMs on silicon wafers negatively affects the veracity of conclusions based on final, steady-state Π_a measurements made at *ca* 1 h analysis time.

2.4. Computation and data representation

Computational, statistical and theoretical methods used in this work have been discussed in detail elsewhere (Vogler 1992*a*,*b*, 1993; Krishnan *et al.* 2003, 2004*b*, 2005*c*). Briefly, time-dependent θ_a data corresponding to protein dilutions (see above) were recovered from TPG files and correlated with concentrations, leading to a matrix of results with row values representing concentration and time (in seconds) as column values. It was, generally, observed that θ_a isotherms were sigmoidal in shape when plotted on logarithmic-concentration axes (Vogler 1992*a*, 1993), with well-defined low-concentration asymptote θ_a^o and high-concentration asymptote θ_a^o (see figure 1). Successive non-linear least-squares fitting of a four-parameter logistic equation $[\theta_a=(\theta_a^o-\theta_a')/(1+(\ln C_B^{\Theta/2}/\ln C_B)^M)+\theta_a']$ to contact angle isotherms data for each time within the observation interval quantified parameters θ_a^o and θ_a' with a measure of statistical uncertainty. Fitting also recovered a parameter measuring concentration-at-half-maximal-change in θ_a, $\ln C_B^{\Theta/2}$ (where $\Theta/2=1/2\Theta^{max}$ and $\Theta^{max}\equiv\theta_a^o-\theta_a'$), as well as a parameter M that measured steepness of the sigmoidal curve. This multi-parameter fitting to concentration-dependent θ_a data was a purely pragmatic strategy that permitted quantification of best-fit protein and surfactant characteristics but is not a theory-based analysis (Vogler 1992*a*,*b*, 1993; Krishnan *et al.* 2003, 2004*b*, 2005*a*). Three-dimensional representations of time-and-concentration-dependent θ_a data were created in Sigma Plot (v.8) from the data matrix discussed above and overlain onto fitted-mesh computed from least-squares fitting. Two-dimensional representations were created from the same data matrices at selected observation times. Measured θ_a were converted to advancing adhesion tension $\tau_a=\gamma_{lv}\cos\theta_a$ for general interpretation (Vogler 1993), where γ_{lv} was the interfacial tension of the contact-angle fluid. Adhesion tensions, $\tau_a^o=\gamma_{lv}^o\cos\theta_a^o$ (pure saline) and $\tau_a'=\gamma_{lv}'\cos\theta_a'$ (at the minimum contact angle observed θ_a') were computed with fitted parameters γ_{lv}^o and γ_{lv}' reported in Krishnan *et al.* (2003, 2004*b*) for the proteins under investigation. Smoothed adhesion–tension isotherms (τ_a versus $\ln C_B$) were computed from smoothed θ_a using smoothed γ_{lv} values computed from best-fit parameters reported in Krishnan *et al.* (2003, 2004*b*). Likewise, smoothed spreading pressure isotherms (Π_a versus $\ln C_B$) were computed from smoothed τ_a curves, where $\Pi_a\equiv(\tau_a-\tau_a^o)$ (table 1).

3. THEORY

3.1. Adsorption isotherms

Adsorption of surface-active solutes (surfactants, where the term includes both synthetic detergents and proteins) can affect LV, SV or SL interfacial tensions, thus producing a change in measured contact angles θ as given by the Young equation $\tau\equiv\gamma_{lv}\cos\theta=\gamma_{sv}-\gamma_{sl}$, where τ is adhesion tension and γ is the interfacial tension at the interface denoted by subscripts. Thus, contact angles can be used to monitor adsorption to solid surfaces (Vogler 1992*a*,*b*, 1993) and citations therein. Contact-angle isotherms are graphical constructions that monitor effects of adsorption by plotting advancing contact angles θ_a against $\ln C_B$ (see figure 1 for examples), where surfactant bulk-phase concentrations C_B range from 10^{-10} to 1% (w/v, see §2). Contact-angle isotherms were sequentially interpreted in terms of adhesion tension (τ_a versus $\ln C_B$) and spreading pressure (Π_a versus $\ln C_B$) isotherms, where $\tau_a\equiv\gamma_{lv}\cos\theta_a$, $\Pi_a=(\tau_a-\tau_a^o)$, γ_{lv} is the LV interfacial tension of the fluid at C_B, and τ_a^o is the adhesion tension of pure buffer ($\gamma_{lv}^o=71.97$ mN m^{-1} at 20 °C). We monitored time dependence of all three isotherm forms but herein interpret only final measurements that achieve or approach steady-state (equilibrium). Issues associated with adsorption reversibility are discussed in §4. Secure interpretation of measured θ_a in terms of τ_a depends on accurate knowledge of γ_{lv} at the bulk-phase surfactant concentration in equilibrium with SL and LV interfaces. Thus, solute depletion of the bulk phase by adsorption may require correction of as-prepared bulk-phase concentration C_B. However, agreement between (uncorrected) tensiometry and instrumental methods of measuring adsorption for surfactants (see table 4) suggests solute-depletion was not a serious issue for surfactant standards. Likewise, for the case of protein adsorption, it can be concluded from a simple calculation that solute depletion was not a serious problem requiring correction (Krishnan *et al.* 2005*c*).

3.2. Gibbs' surface excess

Practical use of concentration-dependent contact angles as a measure of adsorption to the SL interface has been discussed at length elsewhere (Vogler 1992*a*,*b*, 1993) and citations therein. Briefly, for the purposes of this paper, the amount of solute adsorbed to SV and SL interfaces is measured by the Gibbs' surface excess quantities Γ_{sv} and Γ_{sl}, respectively, in units of

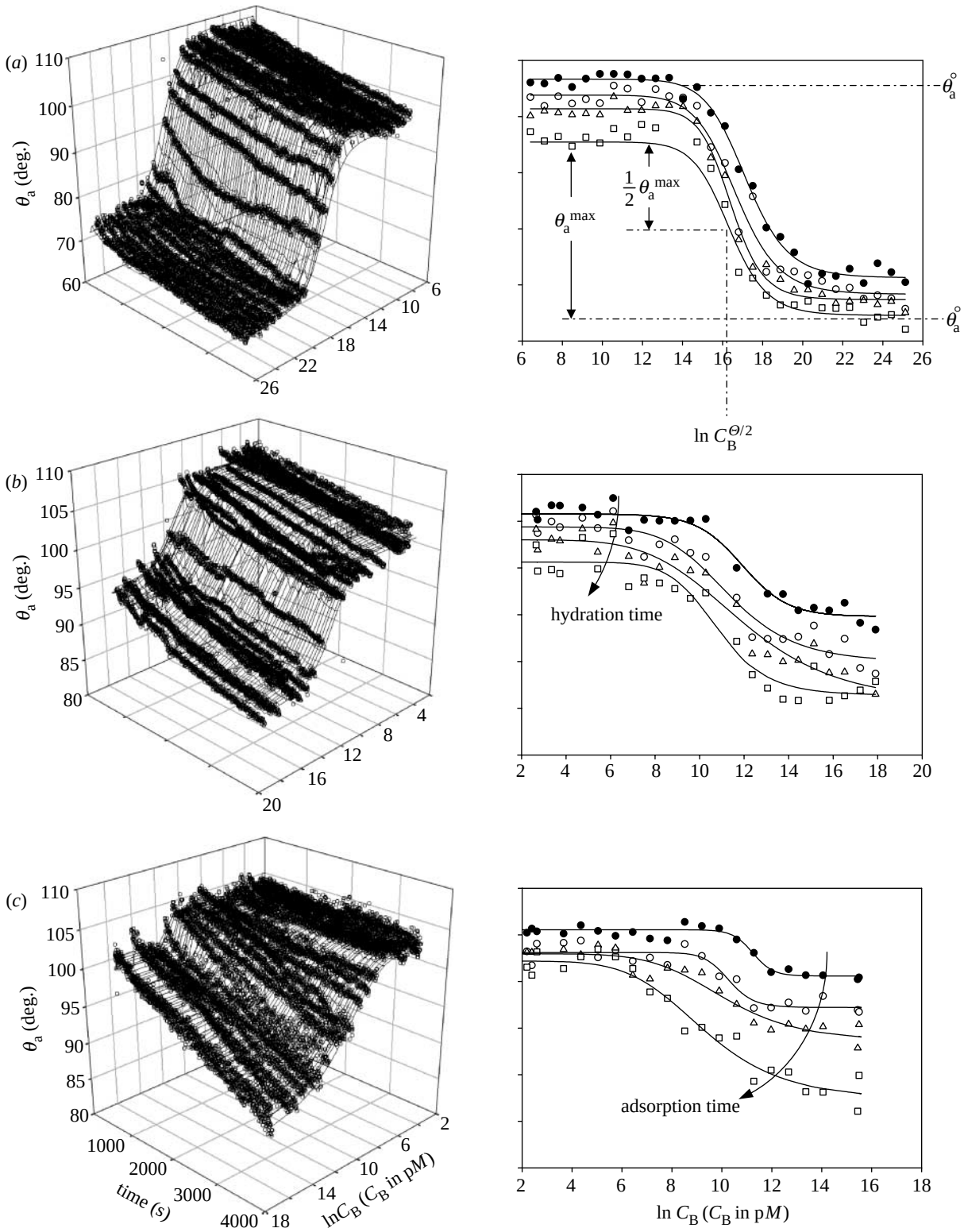

Figure 1. Advancing contact angle isotherms in three-dimensional (θ_a as a function of analysis time (drop age) and logarithmic (natural) solution concentration C_B) and two-dimensional (θ_a as a function of logarithmic solution concentration C_B at selected times) formats comparing Tween-20 (panel *a*,TWEEN-20, table 3), prothrombin (panel *b*, FII, table 3) and immunoglobulin-M (panel *c*, IgM, preparation 2, table 3) adsorption to a methyl-terminated SAM surface. In each case, solute concentration C_B is expressed in pmol l^{-1} (pM) on a natural logarithmic scale. Symbols in two-dimensional panels represent time slices through three-dimensional representations (filled circle = 0.25 s, open circle = 900 s, filled triangles = 1800 s and open triangles = 3594 s; annotations in panel *a* indicate maximum and half-maximum contact angle reduction, θ_a^{max} and $(1/2)\theta_a^{max}$, respectively. Notice that adsorption kinetics dominated IgM adsorption whereas steady-state was achieved within about 1000 s for FII, and nearly no adsorption kinetics is detected for Tween-20. Note also decrease in θ_a° with time, attributed to slow hydration of the SAM surface (panel *b*, arrow annotation; see §4 for more discussion).

Table 1. Glossary of symbols.

C_B	bulk solution concentration (mol/volume)
C_B^{max}	bulk solution concentration at limiting interfacial tension or contact angle (mol/volume)
C_I	interphase concentration (mol/volume)
C_I^{max}	maximal interphase concentration (mol/volume)
$C_B^{\Theta/2}$	bulk solution concentration at half-maximal-change in contact angle (mol/volume)
C_{sl}	independent measure of protein adsorption
χ	proportionality constant, $\chi \equiv R/r_v$
ε	packing efficiency
ΔG^o_{ads}	free energy of protein adsorption
γ_{lv}	liquid–vapour (LV) interfacial tension (mN m^{-1})
γ_{sl}	solid–liquid (SL) interfacial tension (mN m^{-1})
γ_{sv}	solid–vapour (SV) interfacial tension (mN m^{-1})
γ^o_{lv}	low-concentration asymptote of a concentration-dependent γ_{lv} curve (mN m^{-1})
γ'_{lv}	high-concentration asymptote of a concentration-dependent γ_{lv} curve (mN m^{-1})
Γ_{lv}	apparent Gibbs' surface excess calculated at the liquid–vapour (LV) interface (moles/area)
$[\Gamma_{sl}-\Gamma_{sv}]$	apparent Gibbs' surface excess calculated at the solid–liquid (SL) interface (moles/area)
M	parameter fitted to concentration-dependent γ_{lv} or θ_a curve
μ	activity-corrected chemical potential
P	partition coefficient, $P \equiv C_I/C_B$
Π_a	advancing spreading pressure (mN m^{-1})
Π_a^{max}	maximum advancing spreading pressure (mN m^{-1})
r_v	protein radius (cm)
R	effective radius (cm), $R \equiv \chi r_v$
RT	product of universal gas constant and Kelvin temperature (ergs mol^{-1})
S	parameter computed from slope of θ_a isotherm $S = (-1/RT)(\Delta\theta_a/\Delta \ln C_B)$ (moles/area)
τ_a	advancing adhesion tension (mN m^{-1})
τ^o_a	low-concentration asymptote of a concentration-dependent τ_a curve (mN m^{-1}); $\tau^o_a = \gamma^o_{lv} \cos\theta^o_a$
τ'_a	high-concentration asymptote of a concentration-dependent τ_a curve (mN m^{-1}); $\tau'_a = \gamma'_{lv}\cos\theta^o_a$
θ_a	advancing contact angle (deg.)
θ^o_a	low-concentration asymptote of a concentration-dependent θ_a curve (deg.)
θ'_a	high-concentration asymptote of a concentration-dependent θ_a curve (deg.)
θ^*_a	advancing contact angle at half-maximal change in θ_a isotherm $\theta^*_a = (\theta^o_a + \theta^o_a)/2$ (deg.)
Ω	total interphase thickness (cm)

moles/area (the subscript 'a' specifying advancing contact angles is not carried in Γ symbology for the sake of notational compactness). The difference $[\Gamma_{sl}-\Gamma_{sv}]$ (but not separate excess parameters) can be computed from data comprising contact-angle isotherms using equation (3.1)

$$[\Gamma_{sl}-\Gamma_{sv}] = -\left\{\frac{[\gamma_{lv}\sin\theta_a]}{RT}\left(\frac{d\theta_a}{d\ln C_B}\right) + [\Gamma_{lv}\cos\theta_a]\right\}, \tag{3.1}$$

where $d\theta_a/d\ln C_B$ is the slope of a contact-angle isotherm. $\Gamma_{lv} = -(1/RT)(d\gamma_{lv}/d\ln C_B)$ is the surface excess at the LV interface determined from separate measurement of concentration-dependent γ_{lv} of the solute under study (Krishnan *et al.* 2003). This form of the Gibbs' adsorption isotherm is appropriate for a single, isomerically pure non-ionizing solute or a polyelectrolyte in swamping salt concentrations of buffer salts (Rosen 1978; Krishnan *et al.* 2003). It is also important to stress that $[\Gamma_{sl}-\Gamma_{sv}]$ and Γ_{lv} values obtained without correcting concentration C_B for solute activity are 'apparent' surface excess values that can substantially deviate from actual surface excess calculated from $(d\theta_a/d\mu)$ and $(d\gamma_{lv}/d\mu)$, where μ is activity-corrected chemical potential (Frommer *et al.* 1968; Strey *et al.* 1999; Krishnan *et al.* 2003). However, previous work suggests that the discrepancy between apparent and actual Γ_{lv} is roughly constant for the proteins of this study and apparent surface excess was about 56× larger than actual surface excess (Krishnan *et al.* 2003). We thus assume that apparent $[\Gamma_{sl}-\Gamma_{sv}]$ is also *ca* 56× larger than actual, activity-corrected surface excess because the ratio $\{[\Gamma_{sl}-\Gamma_{sv}]/\Gamma_{lv}\} \sim 1$ (see below). Comparison to instrumental measures of adsorption confirms this factor (see table 4).

For relatively hydrophobic surfaces exhibiting $\theta_a > 60°$ and under experimental conditions that avoid inadvertent mechanical deposition of solute at the (SV) interface, as through drop movement on the surface or evaporation for examples, it has been shown that $\Gamma_{sv} \sim 0$ and $[\Gamma_{sl}-\Gamma_{sv}] \rightarrow \Gamma_{sl}$ (Vogler 1992*a*,*b*, 1993). Under the additional restrictions that: (i) solute activities at SL and LV interfaces are approximately equal and (ii) $\Gamma_{sl} \sim \Gamma_{lv}$, it can be expected that $\{[\Gamma_{sl}-\Gamma_{sv}]/\Gamma_{lv}\} \sim 1$. Experimental results confirm that these stringent physical conditions prevail and it is, therefore, concluded that apparent $[\Gamma_{sl}-\Gamma_{sv}] \sim \Gamma_{sl}$ for proteins reported herein.

3.3. Theory of protein adsorption

Previous work disclosed a theory of protein adsorption to the LV surface (Krishnan *et al.* 2003) that appears to be directly applicable to adsorption to the SL surface with little-or-no modification because apparent $[\Gamma_{sl}-\Gamma_{sv}]$ can be directly interpreted in terms of Γ_{sl},

JOURNAL OF THE ROYAL SOCIETY Interface
JOURNAL OF THE ROYAL SOCIETY Interface

Table 2. Purified proteins and surfactants.

name of protein/surfactant (acronym)		molecular weight (kDa)	as-received form (mg ml^{-1})	purity (electrophoresis) or activity	physiologic concentration, mg/100 ml (nominal value)	vendor
ubiquitin (Ub)	prep 1	10.7	powder	98%	10–20 (15)	Sigma Aldrich
	prep 2			95%		EMD Biosciences
thrombin (FIIa)		35.6	powder	1411 NIH units mg^{-1}	n/a	Sigma Aldrich
human serum albumin	prep 1	66.3	powder	98%	3500–5500 (4500)	MP Biomedicals
fraction V (FV HSA)	prep 2		powder	98%		
prothrombin (FII)		72	powder	7.5 units mg^{-1} protein	5–10 (7.5)	Sigma Aldrich
factor XII (FXII)	prep 1	78	solution (2.1)	95%	(4)	Hematologic Technologies
	prep 2		solution (5.5)			
human IgG (IgG)		160	powder	97%	800–1800 (1300)	Sigma Aldrich
fibrinogen (Fb)		340	powder	70% clottable protein	200–450 (325)	Sigma Aldrich
complement component C1q (C1q)		400	solution (1.1)	single band by immunoelectrophoresis	10–25 (17.5)	Sigma Aldrich
α_2-macroglobulin (α mac)	prep 1	725	powder	98%	150–350 (250)	Sigma Aldrich
	prep 2					Sigma Aldrich
	prep 3					MP Biomedicals
human IgM (IgM)	prep 1	1000	solution (0.8)	98%	60–250 (155)	Sigma Aldrich
	prep 2		solution (5.1)	single band by immunoelectrophoresis		MP Biomedicals
sodium dodecyl sulphate (SDS)		0.28	powder	n/a	n/a	Sigma Aldrich
Tween-20 (TWN20)		1.23	neat	n/a	n/a	Sigma Aldrich

JOURNAL OF THE ROYAL SOCIETY Interface
JOURNAL OF THE ROYAL SOCIETY Interface

Table 3. Steady-state protein adsorption parameters.

name of protein/surfactant (acronym)		θ'_a (deg.)	θ^o_a (deg.)	ln $C_B^{\Theta/2}$ PPT (pM)	M (dimensionless)	τ^o_a (mN m^{-1})	τ'_a (mN m^{-1})	Π^{max}_a (mN m^{-1})	ln C_B^{max} (pM)
ubiquitin (Ub)[a]	prep 1	100.9±0.5	75	19 (17)	—	−14	7	21	19
	prep 2	102.2±0.9	75	19 (17)	—	−15	12	27	19
thrombin (FIIa)		99.8±0.5	84.6±0.9	17.5±0.2 (13.9±0.2)	−25.0±8.5	−12.3±0.6	4.5±0.7	16.7±0.9	15.1±0.2
human serum albumin FV HSA	prep 1	103.3±0.8	88.3±0.8	15.9±0.3 (11.7±0.3)	−14.1±5.7	−16.3±0.9	1.4±0.6	17.7±1.2	13.6±0.3
	prep 2	104.5±0.8	88.5±0.6	15.7±0.3 (11.5±0.3)	−11.6±3.0	−17.7±0.9	1.2±.5	18.9±1.1	13.7±0.3
prothrombin (FII)		100.6±0.5	86.5±0.9	15.1±0.4 (10.8±0.4)	−10.1±2.7	−12.9±0.6	2.6±0.7	15.6±0.9	13.2±0.4
factor XII[a]	prep 1	102.9±0.5	94.8±1.0	15.6±0.5 (11.3±0.5)	−17.9±1.2	−15.6	−3.1	12.5	12.7±0.5
	prep 2	102.0±0.4	88.2±0.8	15.7±0.4 (11.3±0.4)	−10.9±3.3	−14.6	1.2	15.8	13.6±0.4
human IgG (IgG)		103.7±0.7	94.9±1.4	15.1±0.9 (10.1±0.9)	−6.9±4.7	−16.8±0.9	−4.4±1.3	12.4±1.5	13.3±0.9
complement component C1q (C1q)		102.6±0.4	95.3±0.7	15.6±0.4 (9.6±0.4)	−12.1±5.6	−15.6±0.5	−5.0±0.7	10.6±0.8	11.4±0.4
α_2-macroglobulin[a] (α mac)	prep 1	101.9±0.5	86	19 (13)	—	−15	4	19	17
	prep 2	100.2±0.9							
	prep 3	103.2±0.5							
human IgM (IgM)	prep 1	102.7±0.6	91.3±1.6	15.5±0.5 (8.7±0.5)	−7.4±2.9	−15.7±0.7	−1.1±1.4	14.6±1.6	11.3±0.5
	prep 2	102.4±0.6	87.8±2.0	15.9±0.6 (9.2±0.7)	−4.9±1.6	−15.4±0.7	1.9±1.7	17.3±1.9	12.6±0.8
sodium dodecyl sulphate (SDS)		100.1±1.9	56.0±2.3	17.7±0.4 (18.9±0.4)	−17.3±4.6	−12.5±2.3	18.7±1.1	31.2±2.6	21.4±0.4
Tween-20 (TWN20)		97.1±0.6	65.1±0.7	16.4±0.3 (16.2±0.1)	−23.4±3.3	−8.9±0.8	14.6±0.5	23.5±0.6	17.8±0.1

[a] Parameters are graphical estimates of fitted parameters (see §4).

JOURNAL OF THE ROYAL SOCIETY Interface
JOURNAL OF THE ROYAL SOCIETY Interface

Table 4. Gibbs' surface excess.

name of protein/surfactant (acronym)		apparent surface excess[a] (pmol cm^{-2})			comparison to literature values		
		$[\Gamma_{sl}-\Gamma_{sv}]$	Γ_{lv}	$\{[\Gamma_{sl}-\Gamma_{sv}]/\Gamma_{lv}\}$	C_{sl} (pmol cm^{-2})	$[\Gamma_{sl}-\Gamma_{sv}]/C_{sl}$	technique (citation)
ubiquitin (Ub)[b]	prep 1	224	179±27	1.3	—	—	—
	prep 2	193		1.1			
thrombin (FIIa)		308±34		1.7±0.3			
human serum albumin FV HAS	prep 1	145±18		0.8±0.2	2.4	60	XR (Sheller *et al.* 1998)
	prep 2	196±21		1.1±0.2		80	
prothrombin (FII)		146±17		0.8±0.2	—	—	—
factor XII[b]	prep 1	136		0.8	—	—	—
	prep 2	153		0.9			
human IgG (IgG)		198±37		1.1±0.3	4.5	44	QCM (Zhou *et al.* 2004)
					2.9	66	SAW (Zhou *et al.* 2004)
complement component C1q (C1q)		117±28		0.7±0.2	—	—	—
α_2-macroglobulin[b] (α mac)	prep 1	130		0.7	—	—	—
	prep 2						
	prep 3						
human IgM (IgM)	prep 1	222±42		1.2±0.3	—	—	—
	prep 2	101±27		0.6±0.2			
sodium dodecyl sulphate (SDS)		276±14	342±10	1.2±0.2	280	0.98	SPR (Sigal *et al.* 1997)
Tween-20 (TWN20)		120±16	455±17	3.8±0.1	120	1.00	SPR (Sigal *et al.* 1997)

[a] Apparent $[\Gamma_{sl}-\Gamma_{sv}]$ or Γ_{lv} is computed without activity correction (see §3).
[b] Parameters are graphical estimates of fitted parameters (see §4).

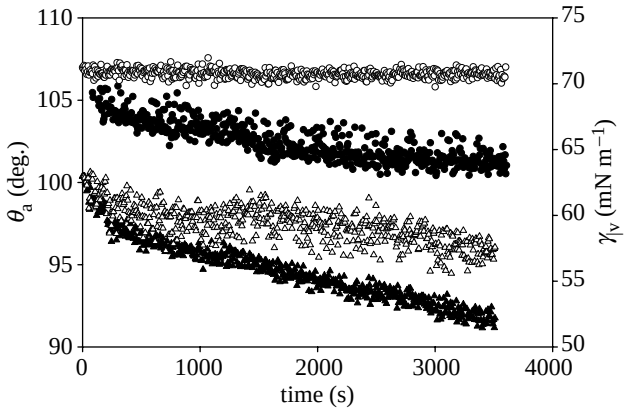

Figure 2. Advancing PBS contact angles θ_a^o (left axis, closed circles) on 1-hexadecane thiol SAMs on gold decrease monotonically with observation time while liquid–vapour interfacial tension, γ_{lv} (right axis, open circles) remains constant, suggesting time-dependent 'hydration' of the SAM surface. SAM hydration also affects θ_a adsorption isotherms shown in figure 1 (arrow annotation, panel *b*). SAM hydration dynamics were separated from protein adsorption kinetics by 'correcting' observed change in θ_a (closed triangles, corresponding to 40 mg ml^{-1} albumin in PBS) for the decrease in θ_a^o observed in control experiments with pure buffer (yielding open triangles).

as discussed above. This protein-adsorption theory was based on two related experimental observations and implications thereof; namely: (i) a surprisingly slight variation in concentration dependence of γ_{lv} among the same diverse globular proteins studied herein (tables 2 and 3) and (ii) a substantially constant, MW-independent value of the apparent Gibbs' surface excess $\Gamma_{lv} = 179 \pm 27$ pmol cm^{-2}. This work demonstrates parallel behaviour at the hydrophobic SL surface with: (i) only modest variation in Π_a isotherms (tables 2 and 3) and (ii) a substantially constant value of the apparent Gibbs' surface excess $[\Gamma_{sl} - \Gamma_{sv}] = 175 \pm 33$ pmol cm^{-2} (table 4, figure 5). Protein adsorption theory asserts that these experimental observations are outcomes of a relatively constant partition coefficient P that entrains protein within a three-dimensional *interphase* separating surface regions from bulk phases (bulk-solution from bulk-vapour for the LV surface or bulk-solution from bulk-solid for the SL surface). This 'Guggenheim' interphase treatment, which is especially relevant to the adsorption of large solutes such as proteins, is to be contrasted with the more familiar two-dimensional *interface* 'Langmuir' paradigm in which the surface is construed to be a planar area with negligible thickness (see Vogler 1998 for more discussion). The three-dimensional interphase is proposed to thicken with increasing protein size because volume occupied by adsorbed-protein molecules scales in proportion to MW according to the well-known relationships among MW, solvent-exposed area, volume, and packing density (Richards 1977). As a consequence of these relationships, molar interphase concentrations C_I of larger proteins are lower than that of smaller proteins at constant $P \equiv C_I/C_B$. In fact, C_I varies inversely with MW and this leads directly to the Traube-rule-like ordering for proteins mentioned in §1. Protein size and repulsion between molecules within the three-dimensional interphase place an upper bound on maximal interphase concentration denoted C_I^{max}. Interphase saturation occurs at C_I^{max} and corresponds to the bulk concentration C_B^{max} at which the limiting adhesion tension τ_a' is achieved (i.e. the concentration at maximum spreading pressure $\Pi_a^{max} = (\tau_a' - \tau_a^o)$). Calibration of theory to neutron-reflectometry (Lu *et al.* 1999) and quasi-electric light scattering (Helfrich 1998; Helfrich & Jones 1999) of albumin adsorbed to the LV surface at C_I^{max} suggests that hydrated spheroidal protein molecules achieve nearly FCC densities or, equivalently, that core proteins pack with an efficiency factor $\varepsilon \sim 0.45$. C_B^{max} is an experimental parameter that can be estimated from concentration-dependent θ_a curves (see appendix A) and is related to C_I^{max} through the partition coefficient $P \equiv C_I^{max}/C_B^{max}$. Equation (3.2) states relationships among packing densities, molecular dimensions (MW), and C_B^{max} in the form of a logarithmic expression that is convenient to apply to concentration-dependent θ_a data:

$$\begin{aligned} \ln C_B^{max} &= \ln(C_I^{max}/P) \\ &= \ln(9.68 \times 10^{11}) - \ln \mathrm{MW} + \ln(\varepsilon/P) \\ &= -\ln \mathrm{MW} + [27.6 + \ln(\varepsilon/P)]. \end{aligned} \tag{3.2}$$

Assuming that ε/P is constant for all proteins within this study, equation (3.2) predicts a linear relationship between $\ln C_B^{max}$ and $\ln \mathrm{MW}$ with a slope of -1 (Krishnan *et al.* 2003). A value for the unknown ratio ε/P can be extracted from the intercept (see §4).

4. RESULTS

4.1. SAM stability

Pure PBS buffer contact angles on SAMs were observed to monotonically decrease with observation time while interfacial tension γ_{lv} (measured by PDT) remained constant, as shown in figure 2 (compare open and closed circles). Specifically, it was observed that θ_a^o of a pure PBS droplet slowly decreased with time from the initial value of $108° < \theta_a^o < 106°$ at $t = 0$ to $104° < \theta_a^o < 102°$ at $t = 1$ h, where θ_a^o is the pure buffer contact angle. The range of reported results corresponds to all 17 methyl-terminated SAM surfaces analysed during the course of this work. This phenomenon attributed to SAM 'hydration' apparently affected time-dependent measurement of protein-solution contact angles because we observed that the whole contact angle isotherm (θ_a versus concentration) slowly shifted lower with time (see figure 1*b*, annotation). Steady-state spreading pressure Π_a isotherms effectively correct for the SAM hydration effect in the adsorption measurement by normalizing to final τ_a^o, that is $\Pi_a = (\tau_a - \tau_a^o)$. A similar strategy was applied to analysis of protein adsorption kinetics, as further illustrated in figure 2 (compare closed triangles and open triangles). At any time t, reduction in pure PBS contact angle due to hydration (closed circles, figure 2) was added to the recorded θ_a for a protein-containing solution (closed

triangles) to 'correct' observed θ_a for the hydration effect (open triangles). This correction procedure typically eliminated the long-term drift in θ_a observed for protein-containing solutions (see filled triangles, figure 2, for example), suggesting that protein adsorption kinetics had, in fact, dampened within the 1 h observation period; as had been generally observed for adsorption of these same proteins at the LV surface (Krishnan *et al.* 2003, 2004*b*).

4.2. General aspects of the data

Table 3 compiles quantitative results of this work. Replicate protein preparations were studied for Ub, FV HSA, FXII, IgM and α_2-macroglobulin. Different vendors were used as a means of controlling for discrepancies that might arise from sourcing (table 2). Contact angle parameters θ_a^o, θ_a', ln $C_B^{\Theta/2}$ and M listed in columns 2–5 of table 3 are the mean fitted values corresponding to final 25 θ_a curves recorded within the 60 min time frame of the TPG experiment. Listed error is standard deviation of this mean. Corresponding adhesion tensions τ_a^o and τ_a' (columns 6 and 7) were computed from θ_a^o and θ_a' values, respectively, with uncertainty estimates computed by propagation of error in θ_a and γ_{lv} measurements (§2). Maximum 'spreading pressure' $\Pi_a^{max} \equiv (\tau_a' - \tau_a^o)$ (column 8) was computed directly from aforementioned τ_a values and associated uncertainty again estimated by propagation of error. Only computed estimates of τ_a^o, τ_a' and Π_a^{max} parameters are provided for FXII since the required γ_{lv} values were graphical estimates (Krishnan *et al.* 2003, 2004*b*). Parameters for ubiquitin and α_2-macroglobulin are also graphical estimates from the steady-state, concentration-dependent θ_a curve since surface saturation was not reached within solubility limits for low-MW proteins at the SL interface (as discussed in appendix C). Therefore, firm values could not be ascertained by statistical-fitting procedures described in §2.

4.3. Adsorption reversibility

Fully reversible adsorption is technically challenging to unambiguously prove. Assumption of reversible adsorption, and hence achievement of thermodynamic equilibrium applied herein, is supported by the following experimental observations.

(i) Concentration-dependent γ_{lv} and θ_a of proteins spanning 3 decades in MW (referred to as 'protein' or 'proteins' below) were like those obtained with small-molecule surfactants in that both followed expectations of Gibbs' adsorption isotherm (Vogler 1992*a*,*b*), with a linear-like decrease in γ_{lv} and θ_a as a function of concentration expressed on a logarithmic concentration axis. Surface excess values (Γ_{lv} and $[\Gamma_{sl} - \Gamma_{sv}]$; see §4*d*) computed from Gibbs' isotherm for surfactant standards agreed with instrumental methods of analysis within experimental error. Surface excess values for proteins adsorbed to LV and SL surfaces were statistically identical.

(ii) Concentration-dependant γ_{lv} and θ_a continuously decreased as a function of solution concentration, well past the concentration required to fill the surface at theoretical monolayer coverage anticipated for irreversible adsorption.

(iii) Proteins were observed to be weak surfactants with a commensurately low partition coefficient deduced from concentration-dependent γ_{lv} and θ_a measurements. Free energy of protein adsorption to hydrophobic LV and SL surfaces calculated from partition coefficients agree with values measured by hydrophobic interaction chromatography (Chen *et al.* 2003).

(iv) Quantitative aspects of protein and surfactant standards adsorbed to hydrophobic LV and SL surfaces were identical within experimental error. Protein adsorption to hydrophobic LV and SL surfaces followed a 'Traube-like' ordering wherein the molar concentration required to achieve an arbitrary spreading pressure decreased in regular progression with MW.

(v) Competitive-protein adsorption experiments at hydrophobic LV and SL surfaces demonstrate protein displacement that follows a simple mass-balance exchange.

These lines of evidence support our contention that protein adsorption was reversible under the experimental conditions applied herein and corroborate the conclusion drawn by other investigators employing very different experimental methods that irreversible adsorption is not an inherent property of proteins (Graham & Phillips 1979; Castillo *et al.* 1985; Brash 1987; Duinhoven *et al.* 1995; Kamyshny *et al.* 2001); see also Vogler (1998) for a review and citations therein.

4.4. Contact-angle isotherms

Time-and-concentration-dependent θ_a for the nonionic surfactant Tween-20 (MW = 1226 Da), and purified proteins, prothrombin (FII; MW = 72 kDa) and IgM (MW = 1000 kDa) are compared in figure 1 in both three-dimensional (θ_a as a function of time and concentration) and two-dimensional (θ_a as a function of concentration at specified times) representations. Note that the logarithmic-solute-concentration ordinate ln C_B in figure 1 is expressed in picomolarity units (pM, 10^{-12} mol solute L^{-1} solution; see §2 for computational and data representation details). Examining first three and two dimensional representations of Tween-20 surfactancy (figure 1*a*) which serves as a reference compound, it was observed that the θ_a curve was sigmoidal in shape, with a well-defined low-concentration asymptote θ_a^o and a high-concentration asymptote θ_a'. In this latter regard, Tween-20 exhibited concentration-limiting behaviour that is typically interpreted as achievement of a critical micelle concentration, at least for surfactants. This paper provides no evidence of

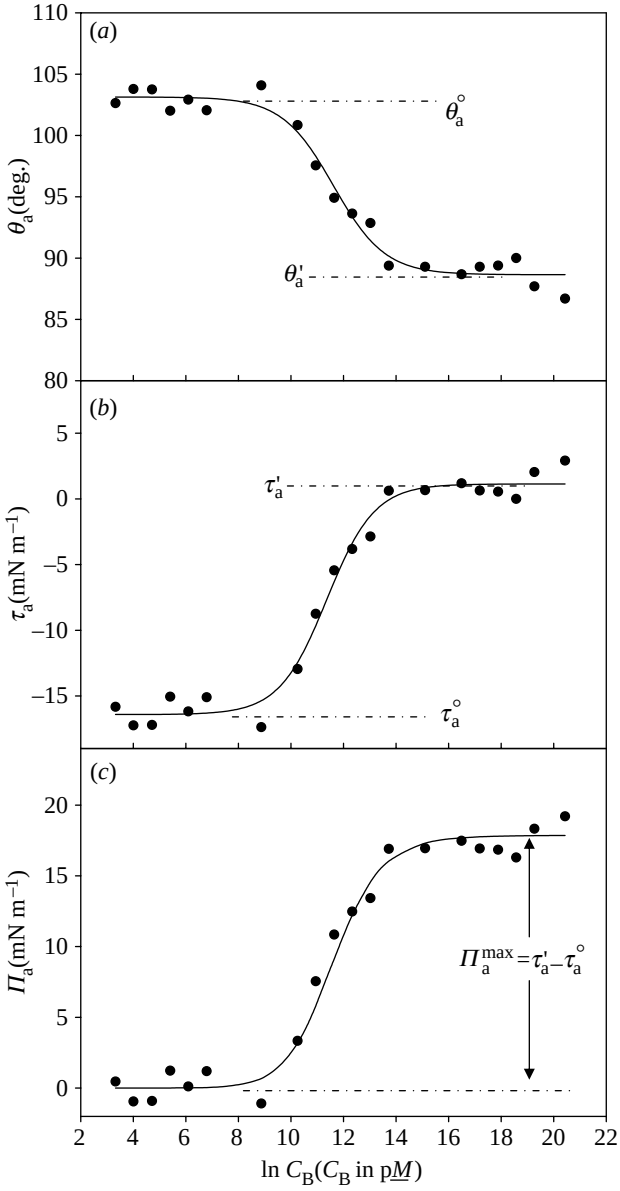

Figure 3. Sequential interpretation of a steady-state (3600 s drop age) contact angle adsorption isotherm for human serum albumin (FV HSA, preparation 2, table 3); panel *a*, advancing contact angles, θ_a; panel *b*, advancing adhesion tension, τ_a; panel *c*, advancing spreading pressure Π_a. Smoothed curves through the data serve as guides to the eye. Annotations identify low- and high-concentration asymptotes for contact angles ($\theta_a^\circ, \theta_a'$), adhesion tensions ($\tau_a^\circ, \tau_a'$) and maximum spreading pressure Π_a^{max} that are used to characterize isotherms (table 3).

micelles, for either proteins or surfactants, and so only acknowledges a limiting behaviour at which further increase in solute concentration did not measurably change θ_a. Smooth curves through the data of figure 1 result from least-squares fitting of the four-parameter logistic equation described in §2.

Results for all proteins were similar to the surfactant standard Tween-20 (as illustrated for FII and IgM in figure 1*b*,*c*, respectively) in that sigmoidal-shaped θ_a isotherms connected low- and high-concentration asymptotes. Significantly more pronounced time dependence in θ_a was observed for proteins, however, especially for intermediate concentrations (in addition

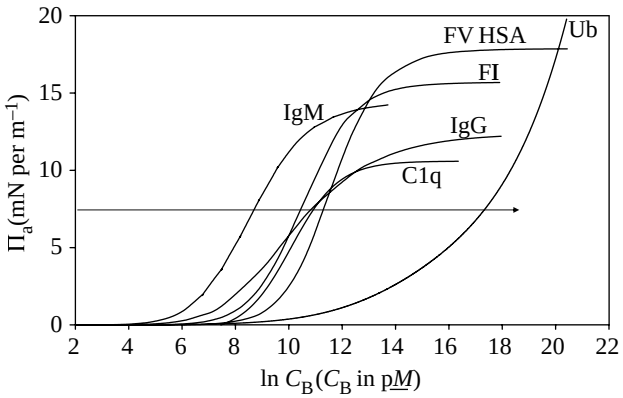

Figure 4. Comparison of steady-state spreading pressure Π_a isotherms for selected proteins spanning three decades in molecular weight (table 2). Smooth curves are guides to the eye (see figures 1 and 3 for similar plots including authentic data and table 3 for statistics of fit). Molar scaling reveals an ordering among diverse proteins, similar to the 'Traube-rule' observed for proteins at the liquid–vapour interface wherein molar concentration required to reach a specified Π_a value decreased with increasing MW (arrow).

to the hydration effects mentioned above). These dynamics were undoubtedly due to rate-limiting, mass-transfer and adsorption steps that slowly brought large macromolecules to LV and SL interfaces relative to the small-molecule reference compound Tween-20 for which only limited dynamics were observed. Observation of time-dependence was important in this particular work only in so far as data demonstrate that θ_a dynamics dampen within the time frame of experimentation, achieving or approaching steady-state (equilibrium) within the 1 h observation window. In fact, data collected in table 3 refers only to steady-state measurements. The bulk-solution concentration at which the limiting θ_a' occurs ($\ln C_B^{max}$) is of theoretical interest in this work and was estimated from fitted parameters compiled in table 3, as described in appendix A.

4.5. Adhesion tension and spreading pressure isotherms

Figure 3 traces sequential interpretation of steady-state (1 h drop age), concentration-dependent θ_a data (panel *a*) in terms of concentration-dependent τ_a (panel *b*) and spreading pressure Π_a (panel *c*) for human serum albumin (FV HSA). Steady-state (equilibrium) spreading pressure isotherms Π_a were used as the basis of comparison of protein adsorption for the compounds listed in table 2. Figure 4 collects Π_a isotherms for selected proteins spanning the molecular weight range $10 < MW < 1000$ kDa showing only smoothed curves for the sake of clarity, but representative θ_a, τ_a and Π_a isotherms with authentic data are amply illustrated in figures 1 and 3. The dynamic range of $\Pi_a \sim 20$ mN m^{-1} was similar to that observed for these proteins at the LV surface and Π_a^{max} fell within a relatively narrow 10 mN m^{-1} band for the diverse set of proteins studied (Krishnan *et al.* 2003). Furthermore, the same 'Traube-rule' ordering of protein adsorption observed at the LV interface was repeated at the SL interface in that

high-MW proteins reduce Π_a to any arbitrary value at lower molarity than low-MW proteins, as suggested by the horizontal arrow annotation on figure 4.

4.6. Apparent Gibbs' surface excess

Adsorption to the SL interface was measured through the apparent Gibbs' excess parameter $[\Gamma_{sl}-\Gamma_{sv}]$ computed using equation (3.1) applied to contact-angle isotherms (see appendix B for example calculations). As noted in §3, the term 'apparent' alerts the reader to the fact that casual application of Gibbs' adsorption isotherm using C_B instead of activity treats solutes (proteins and surfactants) as isomerically pure, non-ionized polyelectrolytes (Frommer & Miller 1968) at infinite dilution with unit activity coefficients (Strey *et al.* 1999). Table 4 collects results for proteins and the small-molecule surfactant standards SDS and Tween-20. Γ_{lv} used in calculation of $[\Gamma_{sl}-\Gamma_{sv}]$ and $\{[\Gamma_{sl}-\Gamma_{sv}]/\Gamma_{lv}\}$ for surfactant standards was 342 ± 10 and 455 ± 17 pmol cm^{-2} for SDS and Tween-20, respectively, and were measured by PDT specifically for this work. $[\Gamma_{sl}-\Gamma_{sv}]$ for proteins were computed using the average $\Gamma_{lv}=179\pm27$ pmol cm^{-2} previously reported to be characteristic of the proteins listed in table 2 (Krishnan *et al.* 2003). Table 4 also lists results of independent measures of adsorption, C_{sl}, for a few of the compounds listed in table 4 to be compared to apparent $[\Gamma_{sl}-\Gamma_{sv}]$ measured by TPG. Note that results for small molecule surfactants SDS and Tween 20 were in good agreement with TPG (i.e. $\{[\Gamma_{sl}-\Gamma_{sv}]/C_{sl}\}\sim0.99\pm0.01$; rows 10, 11 column 6). However, results for proteins (rows 1–9, column 6) were in substantial disagreement (i.e. $\{[\Gamma_{sl}-\Gamma_{sv}]/C_{sl}\}=62.5\pm14.9$). Figure 5 shows that MW dependence of apparent $[\Gamma_{sl}-\Gamma_{sv}]$ (panel *a*) and Γ_{lv} (panel *b*) as well as the ratio $\{[\Gamma_{sl}-\Gamma_{sv}]/\Gamma_{lv}\}$ (panel *c*) was flat for proteins listed in table 2 yielding $\{[\Gamma_{sl}-\Gamma_{sv}]/\Gamma_{lv}\}\sim1$ (see §3).

4.7. A Traube-rule-analogue for protein adsorption and partition coefficient

Figure 6 plots ln C_B^{max} data compiled in table 3 for proteins at the SL interface (panel *a*), and compares with results from the LV interface collected in panel *b* (Krishnan *et al.* 2003, 2004*b*) on natural logarithmic coordinates compatible with equation (3.2) of §3 (data corresponding to ubiquitin was estimated as described in appendix C). Protein data fell within a monotonically decreasing band, generally, consistent with the anticipation of a unit slope and positive intercept [$\ln C_B^{max}=(-1.3\pm0.2)\ln \mathrm{MW}+(19.8\pm1.0)$; $R^2=78\%$]. Comparison to equation (3.2) revealed that $\varepsilon/P\sim4.1\times10^{-4}$ from the nominal intercept value and, by assuming $\varepsilon\sim0.45$ (as discussed in §3), estimated $P\sim1100$.

4.8. Competitive protein adsorption

We have observed that τ'_a for all of the diverse proteins studied herein fell within a relatively narrow 10 mN m^{-1} band. However, no two proteins were found to be identical in this regard, mirroring results obtained for these same proteins adsorbed to the hydrophobic LV surface (Krishnan *et al.* 2003, 2004*a*,*b*). In fact, we found that this 'interfacial signature' could be used as a kind of tracer in competitive-adsorption experiments revealing the composition of the interphase formed by adsorption from binary protein mixtures. These mixing experiments also demonstrate that one protein can displace another, strongly indicating that proteins were not irreversibly adsorbed to the surface. Figure 7 examines time-dependent adhesion tension and spreading pressure of hIgM and FV HSA solutions mixed in various proportions at a fixed total protein concentration of 5 mg ml^{-1}; see Krishnan *et al.* (2004*b*) for more details of HSA and IgM interfacial properties. Protein-adsorption kinetics led to time-dependent τ_a (corrected for SAM hydration, see above) wherein adhesion tension was observed to quickly rise from $\tau_a^o\sim-20$ mN m^{-1} characteristic of pure PBS on the SAM surface to a steady-state (equilibrium) τ'_a characteristic of that protein solution, as illustrated in figure 7*a* for 100% albumin (circles), 50 : 50 albumin : IgM (diamonds), and 100% IgM (squares). Figure 7*b* plots observed steady-state (1 h) spreading pressure Π_{obs} at varying weight-fraction albumin compositions f_{alb} in hIgM (expressed as percent of 5 mg ml^{-1} total protein). These results strongly suggest that competitive adsorption between proteins leads to displacement of hIgM by albumin through a process that strictly follows the wt/v concentration of competing proteins and clearly indicate that IgM was not irreversibly adsorbed.

5. DISCUSSION

5.1. Adsorption isotherms

Adsorption isotherms constructed from concentration-dependent contact angles (θ_a, τ_a and Π_a, see figures 1, 3 and 4) for the proteins studied herein exhibited many similarities to concentration-dependent γ_{lv} reported previously (Krishnan *et al.* 2003). Maximum spreading pressure, Π_a^{max}, fell within a relatively narrow $10<\Pi_a^{max}<20$ mN m^{-1} band characteristic of all proteins studied, just as observed at the LV surface. Furthermore, Π_a isotherms exhibited the 'Traube-rule-like' progression in MW observed at the LV surface wherein the molar concentration required to reach a specified Π_a value decreased with increasing MW. Bearing in mind the great range in MW spanned by proteins in figure 4, it is reasonable to conclude that commensurate variability in protein composition did not confer widely varying SL interfacial activity; at least not in comparison to the full range available to ordinary surfactants. The inference taken from the Traube-rule-like progression is that protein concentration required to reduce Π_a to a specified value decreases with MW in a manner loosely consistent with the addition of a generic amino-acid-building-block having an 'average amphilicity' that increases MW but does not radically change protein amphilicity. Otherwise, if MW increased by addition of amino-acid-building-blocks with highly variable amphilicity, then Π_a would be expected to be a much stronger function of protein MW than is observed. Thus, it appears that molar variability in Π_a is achieved by aggregating

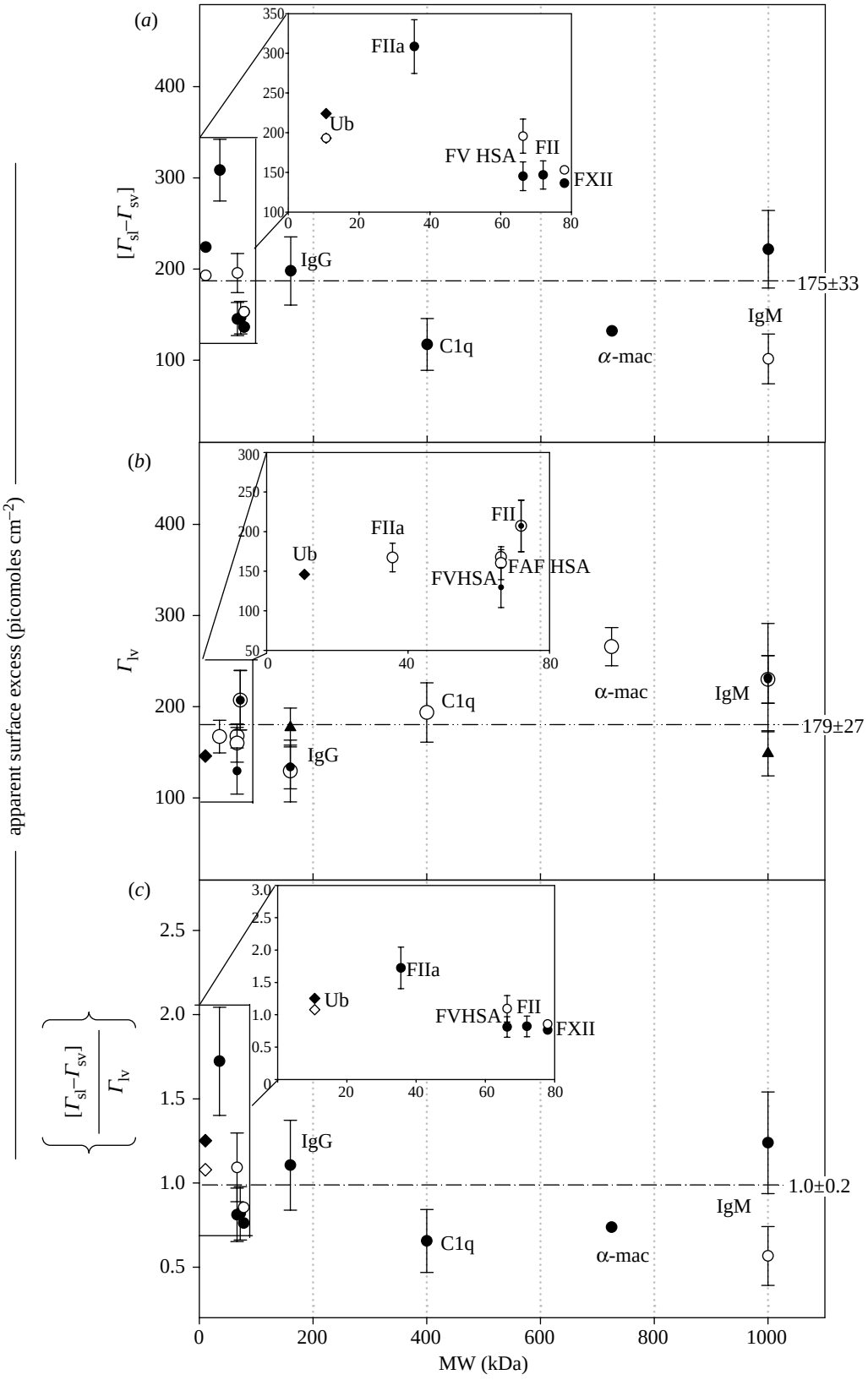

Figure 5. Apparent Gibbs' surface excess scaled by protein MW at the solid–liquid (SL) ($[\Gamma_{sl}-\Gamma_{sv}]$, panel *a*) and the liquid–vapour (LV) interfaces (Γ_{lv}, panel *b*) for multiple protein preparations (open circle = preparation 1, filled circle = preparation 2, filled triangle = preparation 3; see tables 2 and 4). Panel *c* plots the ratio of the surface excess parameters yielding $\{[\Gamma_{sl}-\Gamma_{sv}]/\Gamma_{lv}\}\sim 1$. Insets expand low-MW region and dashed lines represent arithmetic mean of the respective surface excess values listed in table 4 (see appendix B for sample calculations). Apparent Γ_{lv} (panel *b*) is reproduced (Krishnan *et al.* 2003) for comparison to $[\Gamma_{sl}-\Gamma_{sv}]$. Apparent surface excess $[\Gamma_{sl}-\Gamma_{sv}]$ and Γ_{lv}, as well as the ratio $\{[\Gamma_{sl}-\Gamma_{sv}]/\Gamma_{lv}\}$, were found to be independent of protein MW (see §§3 and 5).

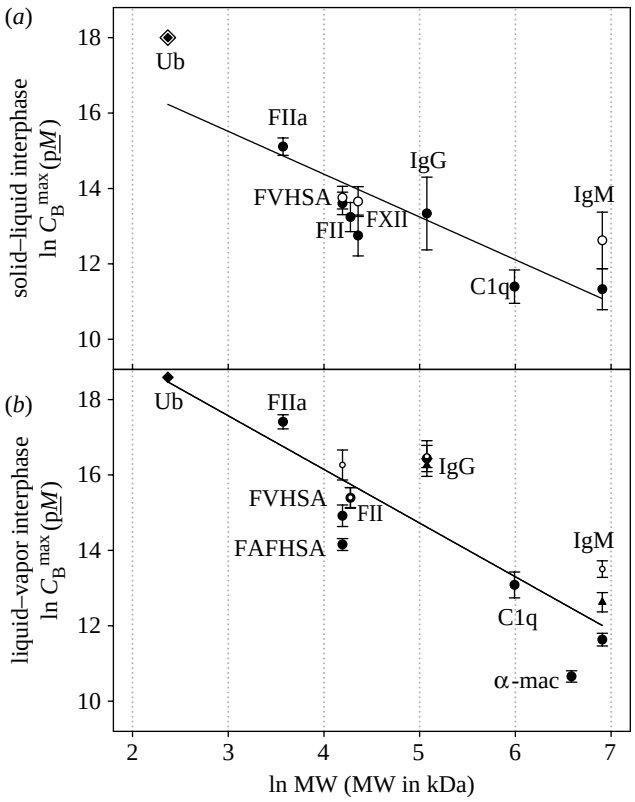

Figure 6. Relationship between the surface-saturating bulk solution concentration C_B^{max} and protein MW (natural logarithmic scale) at the solid–liquid (SL, panel *a*) and liquid–vapour interfaces (LV, panel *b*) for multiple protein preparations (open circle = preparation 1, filled circle = preparation 2, filled triangle = preparation 3). Error bars represent uncertainty computed by propagation of experimental errors into compiled ln C_B^{max} values (see table 3 and appendix A for representative calculations). Panel *b* is reproduced from (Krishnan *et al.* 2003) for the purpose of comparing the LV and SL interfaces. Linear regression through the SL data yielded $[\ln C_B^{max} = (-1.3 \pm 0.2) \ln \mathrm{MW} + (19.8 \pm 1.0);\ R^2 = 78\%]$ compared to $[\ln C_B^{max} = (-1.4 \pm 0.2) \ln \mathrm{MW} + (21.8 \pm 1.3);\ R^2 = 72\%]$ for the LV interface, consistent with the expectation of unit slope and a positive intercept (see §§3 and 5). Note that low-MW proteins require greater bulk-phase concentrations to saturate the interphase than higher-MW proteins.

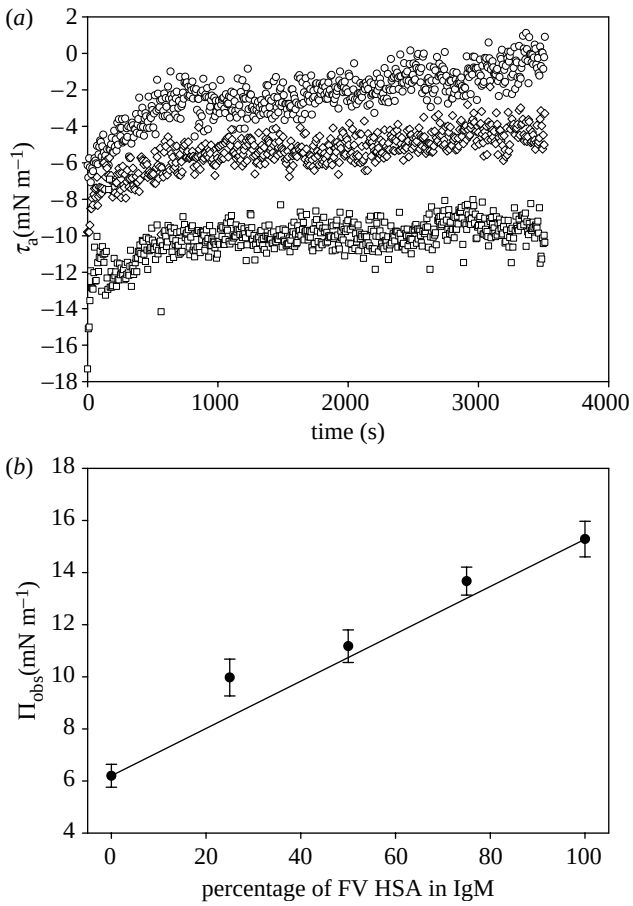

Figure 7. Time-dependent adhesion tension τ_a (panel *a*) of pure albumin (circles), pure hIgM (squares), and a 50 : 50 mixture of albumin in hIgM (diamonds) at constant 5 mg ml^{-1} total protein. Note that τ_a of the 50 : 50 mixture fell between the pure protein solutions. Observed spreading pressure Π_{obs} (panel *b*) followed a simple linear combining rule expressed in weight-fraction protein in the bulk phase $\Pi_{obs} = \Pi_{alb} - f_{IgM}(\Delta\Pi)$, where $\Delta\Pi = (\Pi_{alb} - \Pi_{IgM})$, Π_{alb} or Π_{IgM} refer to Π_{obs} at 100% albumin ($f_{IgM} = 0$) or 100% IgM ($f_{IgM} = 1$), respectively. Error bars represent standard deviation of the mean of the final 25 Π_{obs} values observed at 1 h equilibration time.

greater mass of similar amphiphilic character, as opposed to accumulating greater amphilicity with increasing MW.

5.2. Apparent Gibbs' surface excess

Adsorption measurements by concentration-dependent contact angles were in good agreement with literature values for the surfactant standards SDS and Tween-20, as listed in table 4. Close agreement between apparent $[\Gamma_{sl} - \Gamma_{sv}]$ and C_{sl} from alternative methods suggests that (i) assumptions of purity and unitary activity coefficients were reasonable for these small molecules and (ii) solute deposition at the SV interface was negligible (see §3). However, $[\Gamma_{sl} - \Gamma_{sv}]$ for proteins were quite different than values drawn from comparable literature sources, as was observed to be the case for apparent Γ_{lv} (Krishnan *et al.* 2003). No doubt proteins violate assumptions of ideality and unitary activity coefficients (Wills *et al.* 1993; Knezic 2002), causing apparent $[\Gamma_{sl} - \Gamma_{sv}]$ to deviate substantially from real, activity-corrected surface excess. Previous work showed that apparent and real Γ_{lv} for proteins were different by a factor of about 56 and that apparent Γ_{lv} was approximately constant across the span of protein MW studied (Krishnan *et al.* 2003). Apparent $[\Gamma_{sl} - \Gamma_{sv}]$ was found to differ from independent measures by a factor of 62.5 ± 14.9, as inferred from the mean $\{[\Gamma_{sl} - \Gamma_{sv}]/C_{sl}\}$ ratio for proteins (see column 6, rows 1–9, table 4), consistent with estimates from the LV interface above. Figure 5 plots apparent $[\Gamma_{sl} - \Gamma_{sv}]$ and Γ_{lv}, and the ratio $\{[\Gamma_{sl} - \Gamma_{sv}]/\Gamma_{lv}\}$ as a function of MW showing that $\Gamma_{lv} \sim [\Gamma_{sl} - \Gamma_{sv}]$ and that, as a consequence, $\{[\Gamma_{sl} - \Gamma_{sv}]/\Gamma_{lv}\} \sim 1$. We thus conclude that $[\Gamma_{sl} - \Gamma_{sv}] \sim \Gamma_{sl} \sim \Gamma_{lv}$ for the globular proteins studied herein. By contrast, $\{[\Gamma_{sl} - \Gamma_{sv}]/\Gamma_{lv}\} = 3.8 \pm 0.1$ for Tween 20 (row 11, column 4, table 4) suggesting nearly 4× concentration at the SL interface over LV, consistent with results reported for Tween-80 at silanated glass surfaces (Vogler 1993).

5.3. A Traube-rule-analogue for protein adsorption and partition coefficient

A flat trend in Γ_{lv} and Γ_{sl} with MW is consistent with an interphase concentration C_I (in units of moles cm^{-3}) scaling inversely with MW and an interphase thickness Ω (in units of cm) that scales directly with MW. This is because $\Gamma = C_I\Omega$ (when the partition coefficient $P \gg 1$) and MW dependence cancels (Krishnan *et al.* 2003). In other words, the interphase thickens as adsorbed proteins become larger and Gibbs' dividing plane descends deeper into the surface region (Vogler 1992*a*, *b*, 1993). Interpreted in terms of the theory of protein adsorption briefly outlined in §3, hydrated spheroidal protein molecules with net radius R scaling as a function of $MW^{1/3}$ pack into the interphase to a concentration C_I^{max} limited by osmotic repulsion between molecules. Or stated another way, C_I^{max} is limited by the extent to which the interphase can be dehydrated by protein displacement of interfacial water. Interphase dehydration is more related to the properties of water than the proteins themselves and so the partition coefficient $P \equiv C_I/C_B$ is observed to be approximately constant among the proteins investigated.

Figure 6*a* plots C_B^{max} data compiled in table 3 on logarithmic coordinates compatible with equation (3.2) of §3. Proteins fell within a monotonically decreasing band roughly consistent with the anticipation of a unit slope and positive intercept [$\ln C_B^{max} = (-1.3 \pm 0.2) \ln MW + (19.8 \pm 1.0)$; $R^2 = 78\%$]. A similar trend was observed for protein adsorption at the LV surface, shown in figure 6*b*. Interpretation of these results must take into account that the highly simplified model of adsorption treats proteins as uniform hard spheres and does not attempt to account for structural complexities of real molecules, or unfolding (denaturation) that may occur upon packing within the surface region. Hence, failure of data to quantitatively adhere to equation (3.2) is hardly surprising. Even so, results for Ub were significantly off the trend obtained at the LV surface (compare to figure 6*a*,*b*), possibly signalling that this small protein does not retain a spherical geometry at the SL surface. Clearly, more work is required to further test such speculation and expand the range of proteins explored. However, even in light of scatter in the data of figure 6*a*, it is of interest to estimate $\varepsilon/P \sim 4.1 \times 10^{-4}$ from the nominal intercept value and, by assuming $\varepsilon \sim 0.45$ (see §3), estimate $P \sim 1100$; which is within an order-of-magnitude of the $P \sim 150$ estimate from analysis of protein adsorption to the LV surface and $P \sim 5000$ from neutron reflectometry of albumin adsorption to the LV surface (Krishnan *et al.* 2003). Clearly, goniometry is not a good method for deducing partition coefficients, but it is of continued interest to compute protein adsorption energetics based on these rough estimates. With $10^2 < P < 10^3$, the free energy of protein adsorption to the hydrophobic surface $\Delta G^o_{ads} = -RT \ln P$ is very modest, lying within the range $-7RT < \Delta G^o_{ads} < -4RT$. This is consistent with estimates for lysozyme, myoglobin, and α-amylase adsorption to hydrophobic surfaces ($\Delta G^o_{ads} \sim -5RT$) measured by hydrophobic interaction chromatography (Chen *et al.* 2003). Thus, a conclusion that can be drawn, in spite of rather poor estimates of P, is that adsorption of proteins to a hydrophobic surface is energetically favourable by only small multiples of thermal energy RT and apparently does not vary significantly among proteins.

According to equation (3.2) and figure 6, low-MW proteins require greater bulk-phase concentrations to saturate the SL (or LV) interphase than higher-MW proteins. Given that C_B^{max} values plotted in figure 6 approach 1 w/v%, it is reasonable to anticipate that extrapolated C_B^{max} values for yet-lower-MW proteins must equal or exceed protein-solubility limits. As a consequence, surface saturation and the related limiting Π_a^{max} is not expected for low-MW proteins at fixed P. In this regard, it is noteworthy that Π_a isotherms for low-MW proteins such as ubiquitin (10.7 kDa) fail to achieve a limiting Π_a^{max} at any concentration below the solubility limit, as was observed for concentration-dependent γ_{lv}.

5.4. Competitive protein adsorption

Figure 7 is strong evidence that there is ready exchange of albumin and IgM at the SAM surface, with relative amounts of adsorbed protein following a simple linear combining rule expressed in weight-fraction protein in the bulk phase. Taken together with related observations summarized in §3, we are led to conclude that protein adsorption to hydrophobic SAM surfaces was substantially reversible under the experimental conditions employed in this work. The word 'substantially' is purposely used here because evidence at hand does not guarantee that every adsorbed protein molecule was reversibly bound to the surface (or within the surface region). Indeed, some unknown fraction of adsorbed protein could be irreversibly bound to surface defects which are undetected by tensiometric methods applied herein. However, given the exquisite quality of SAM surfaces and similarity of results obtained at molecularly smooth LV surfaces, this putative fraction of irreversibly bound protein must be vanishingly small.

6. CONCLUSIONS

Interfacial energetics of protein adsorption from aqueous-buffer solutions to hydrophobic methyl-terminated SAM surfaces are strikingly similar to the interfacial energetics of protein adsorption to the hydrophobic air–water surface. The observed Traube-rule-like progression in interfacial-tension reduction (γ_{lv} and τ_a), conserved partition coefficient P, and constant Gibbs' surface excess (Γ_{lv} and Γ_{sl}) for globular proteins spanning three decades in MW all occur because water controls the energetics of the adsorption process. Hence, protein adsorption to hydrophobic surfaces has more to do with water than the proteins themselves. A relatively straightforward theory of protein adsorption predicated on the interfacial packing of hydrated spherical molecules with dimensions scaling as a function of MW accounts for the essential physical chemistry of protein adsorption and rationalizes significant experimental observations. From this theory it is evident that displacement of interfacial

water by hydrated proteins adsorbing from solution places an energetic cap on protein adsorption to hydrophobic surfaces ($-7RT < \Delta G^{o}_{ads} < -4RT$). This phenomenon is generic to all proteins. Thus, globular–blood protein adsorption to hydrophobic surfaces is not found to significantly vary among diverse protein types.

Variations from general trends discussed above may reflect deviations in protein geometry from simple spheres and/or tendency of some proteins to adopt a more spread/compact configuration (denature) in the adsorbed state. Indeed, there is the expectation from a burgeoning literature base that proteins 'denature' over time (Birdi 1989). Denaturation can include changes in molar free volume/interfacial area, loss of higher-order structure with concomitant change in specific bioactivity, and irreversible adsorption. Of course, tensiometric methods are effectively blind to these molecular processes, except insofar as denaturation may lead to time-varying interfacial tensions and contact angles. Our measurements achieved, or asymptotically approached, a well-defined steady-state within the hour observation window applied, suggesting that putative 'denaturation processes' either had an insignificant impact on results or occurred significantly faster/slower than the time frame of experimentation. Given the similarity in adsorption energetics to hydrophobic LV and SL surfaces among the broad array of proteins studied and the general expectation that denaturation is a slow process, we are inclined to conclude that either denaturation did not significantly affect results (perhaps accounting for small-but-measurable differences among proteins) or the denaturation effect was astonishingly similar among very different proteins. With regard to irreversible adsorption, we note that experiments examining competitive adsorption between albumin and IgM at the LV surface demonstrated protein displacement (Vroman effect) that followed a simple mass-balance exchange (Krishnan *et al.* 2004*a*), strongly suggesting that neither albumin nor IgM was irreversibly adsorbed to this surface.

This work was supported, in part, by the National Institute of Health PHS 5 R01 HL 69965-03, by Johnson & Johnson through the Focused Giving Grant Program, and a grant with the Pennsylvania Department of Health. The Department Pennsylvania Department of Health specifically disclaims responsibility for any analyses, interpretations or conclusions. The authors appreciate additional support from the Materials Research Institute and Departments of Bioengineering and Materials Science and Engineering, Penn State University. The authors gratefully acknowledge the assistance of Dr Roger Woodward in instrument design and implementation. This is a contribution from the Hematology at Biomaterial Interfaces Research Group.

APPENDIX A. ESTIMATION OF C_B^{max}

C_B^{max} was calculated from the slope of an advancing contact angle θ_a isotherm $\Delta\theta_a/\Delta \ln C_B$ and fitted data (table 3) by evaluating equation (A 1) at half-maximal change in θ_a, which occurs at a bulk-phase composition $\ln C_B^{\Theta/2}$ (where $\Theta/2 = 1/2\Theta^{max}$ and $\Theta^{max} \equiv \theta_a^o - \theta_a'$)

$$\Delta\theta_a/\Delta \ln C_B = -RTS = \frac{(\theta_a' - \theta_a^*)}{[\ln C_B^{max} - \ln C_B^{\Theta/2}]}$$

$$= \frac{(\theta_a' - (\theta_a^o + \theta_a^o/2))}{[\ln C_B^{max} - \ln C_B^{\Theta/2}]}$$

$$\Rightarrow \ln C_B^{max} = \frac{\Theta^{max}}{2RTS} + \ln C_B^{\Theta/2}, \quad \text{(A 1)}$$

where the terms $S \equiv -(1/RT)(\Delta\theta_a/\Delta \ln C_B)$, $\theta_a^* \equiv \theta_a$ measured at $\ln C_B^{\Theta/2}$ and $\Theta^{max} \equiv \theta_a^o - \theta_a'$. All of the parameters in the RHS of equation (A 1) are derived from non-linear, least-squares fitting of θ_a isotherms to the four-parameter logistic equation described in §2. Confidence in C_B^{max} values listed in table 3 and plotted in figure 6 was computed by propagation of the standard errors in best-fit parameters through equation (A 1), as given by equation (A 2). In consideration of all sources of experimental error, we conclude that $\ln C_B^{max}$ estimates are no better than about 20%.

$$\sigma^2_{\ln C_B^{max}} = \sigma^2_{\ln C_B^{\Theta/2}} + \frac{1}{4(RTS)^2}\left[\sigma^2_{\theta_a^o} - \sigma^2_{\theta_a'} - \left(\frac{\theta_a^o - \theta_a'}{S^2}\right)^2 \sigma_S^2\right], \quad \text{(A 2)}$$

where σs represent standard errors in $\ln C_B^{max}$ and the best-fit parameters $\ln C_B^{\Theta/2}$, θ_a^o, θ_a' and S as denoted by subscripts.

APPENDIX B. ESTIMATION OF $[\Gamma_{SL} - \Gamma_{SV}]$

The apparent Gibbs' surface excess $[\Gamma_{sl} - \Gamma_{sv}]$ was computed from equation (3.1) of §3 for each of the proteins and surfactants listed in table 4. The following steps illustrate surface excess calculations for FV HSA (preparation 1, table 3) at the SL interface. Fit of θ_a isotherm data plotted in figure 3 yielded $\theta_a^o = 103.3 \pm 0.8$, $\theta_a' = 88.3 \pm 0.8$, $\ln C_B^{\Theta/2} = 15.9 \pm 0.3$ and $M = -14.1 \pm 5.7$. Inflections in the θ_a curve were located at $X_1 = 13.7$ and $X_2 = 10.9$ (dimensionless), yielding a slope estimate S' from the finite difference with calculated uncertainty as $S' \equiv \Delta\theta_a/\Delta X = -2.95 \pm 0.04$ deg $= -0.050 \pm 0.007$ rad, where $\Delta\theta_a = \theta_a|_{X_2} - \theta_a|_{X_1}$ and $\Delta X = X_2 - X_1$. Values for θ_a were calculated from the characteristic parameters above, conveniently evaluated at $\ln C_B = \ln C_B^{\Theta/2}$, where the logistic equation simplifies to $\theta_a = \theta_a^* = (\theta_a^o + \theta_a')/2$. Thus, $\theta_a^* = (103.3 + 88.3)/2 = 95.8°$; $\sin\theta_a^* = 0.99$; and $\cos\theta_a^* = -0.10$. The required term γ_{lv} was calculated from a comparable logistic equation for γ_{lv} isotherms, using LV fitted parameters (Krishnan *et al.* 2003, 2004*b*), but evaluated at $\ln C_B = \ln C_B^{\Theta/2} = 11.7$ as

$$\left[\gamma_{lv} = \frac{70.8 - 46.2}{1 + (12.4/11.7)^{-7.3}} + 46.2\right] = 61.1 \text{ mN m}^{-1}.$$

Using $\Gamma_{lv}=179$ pmol cm^{-2} determined from Krishnan *et al.* (2003), equation (3.1) was computed as

$$[\Gamma_{sl}-\Gamma_{sv}] = -\left\{\frac{[61.1\sin 95.8]\text{ergs cm}^{-2}}{(8.31\times10^{7})(298.15)(10^{-12})\text{ergs pmol}^{-1}}(-0.05) + [179\cos 95.8]\right\} = 145\text{ pmol cm}^{-2}.$$

Uncertainty in $[\Gamma_{sl}-\Gamma_{sv}]$ was computed by propagation of error into $\Delta\Gamma=[\Gamma_{sl}-\Gamma_{sv}]$ as

$$\sigma^2_{\Delta\Gamma} = \left[\frac{\sin\theta_a}{RT}\frac{d\theta_a}{d\ln C_B}\right]^2\sigma^2_\gamma + \left[\frac{\gamma_{lv}}{RT}\frac{d\theta_a}{d\ln C_B}\cos\theta_a+\Gamma_{lv}\sin\theta_a\right]^2\sigma^2_\theta + \left[\frac{\gamma_{lv}\sin\theta_a}{RT}\right]^2\sigma^2_{S'}+\sigma^2_{\Gamma_{lv}}\cos^2\theta_a, \quad \text{(B 1)}$$

where $S'\equiv d\theta_a/d\ln C_B$. The σ terms for γ_{lv}, θ_a and S' were computed from $\sigma^2_{\gamma_{lv}}=(\sigma^2_{\gamma^o_{lv}}+\sigma^2_{\gamma'_{lv}})/4$ and $\sigma^2_{\theta_a}=(\sigma^2_{\theta^o_a}+\sigma^2_{\theta'_a})/4$, where γ^o_{lv}, γ'_{lv} and θ^o_a, θ'_a are fitted parameters from γ_{lv} and θ_a isotherms; as described above. Uncertainty in slope $\sigma^2_{S'}=(\sigma^2_{\theta^o_a}+\sigma^2_{\theta'_a})/\Delta X^2$. Thus, uncertainty in $\Delta\Gamma$ is given by

$$\sigma^2_{\Delta\Gamma} = \left[\frac{\sin 95.8}{(2.48\times10^{-2})}(-0.05)\right]^2(1.88) + \left[\frac{61.1\sin 95.8}{(2.48\times10^{-2})}\right]^2(5.1\times10^{-5})+(27)^2\cos^2 95.82 + \left[\frac{61.1}{(2.48\times10^{-2})}(-0.05)\cos 95.8+179\sin 95.8\right]^2 \times(9.8\times10^{-5}) = 324.95,$$

$$\sigma_{\Delta\Gamma} = 18.02,$$

where $RT=(8.31\times10^7)(298.15)(10^{-12})=2.48\times10^{-2}$ergs pmol^{-1}. Thus, $[\Gamma_{sl}-\Gamma_{sv}]=145\pm18$ pmol cm^{-2} as reported in table 4 (row 4 column 2).

APPENDIX C. ESTIMATION OF PARAMETERS FOR UBIQUITIN AND α_2-MACROGLOBULIN

Parameters for ubiquitin and α_2-macroglobulin listed in tables 3 and 4 and shown in figures 4–6 were graphical estimates from the steady-state, concentration-dependent θ_a curve. Firm values could not be ascertained by statistical-fitting procedures described in §2 because surface saturation was not reached within solubility limits for this protein. Thus, well-defined high concentration asymptotes, θ'_a were not achieved at physically realizable concentrations. Hence, θ_a measured at the highest-concentration studied was used as an estimate for θ'_a. Adhesion tensions were computed accordingly, with graphical estimates from γ_{lv} isotherm as $\tau^o_a=\gamma^o_{lv}\cos\theta^o_a$ and $\tau'_a=\gamma'_{lv}\cos\theta'_a$. $\ln C_B^{\Theta/2}$ and $d\theta_a/d\ln C_B$ parameters were estimated by graphical location of inflection points on the θ_a curve. These estimates were used in the calculation of C_B^{max} and $[\Gamma_{sl}-\Gamma_{sv}]$ parameters, as described in appendices A and B.

REFERENCES

Allara, D. L. & Nuzzo, R. G. 1985 Spontaneously organized molecular assemblies. 2. Quantitative infrared spectroscopic determination of equilibrium structures of solution-adsorbed *n*-alkanoic acids on an oxidized aluminum surface. *Langmuir* **1**, 52–66. (doi:10.1021/la00061a008)

Birdi, K. S. 1989 *Lipid and biopolymer monolayers at liquid interfaces*, vol. 10. New York: Plenum Press.

Brash, J. L. 1987 Protein adsorption at the solid-solution interface in relation to blood-material interactions. In *Proteins at interfaces: physicochemical and biochemical studies* (ed. J. L. Brash & T. A. Horbett). ACS Symposium Series, vol. 343, pp. 490–506. Washington, DC: American Chemical Society.

Brynda, E., Cepalova, N. & Stol, M. 1984 Equilibrium adsorption of human serum albumin and human fibrinogen on hydrophobic and hydrophilic surfaces. *J. Biomed. Mater. Sci.* **18**, 685–693. (doi:10.1002/jbm.820180609)

Castillo, E., Koenig, J. & Anderson, J. 1985 Protein adsorption on hydrogels. II. Reversible and irreversible interactions between lysozyme and soft contact lens surfaces. *Biomaterials* **6**, 338–345. (doi:10.1016/0142-9612(85)90089-4)

Chalikian, T. V. & Breslauer, K. J. 1996 On volume changes accompanying conformational transitions of biopolymers. *Biopolymers* **39**, 619–626. (doi:10.1002/(SICI)1097-0282(199611)39:5<619::AID-BIP1>3.0.CO;2-Z)

Chen, W.-Y., Huang, H.-M., Lin, C.-C., Lin, F.-Y. & Chan, Y.-C. 2003 Effect of temperature on hydrophobic interaction between proteins and hydrophobic adsorbents: studies by isothermal titration calorimetry and the van't Hoff equation. *Langmuir* **19**, 9395–9403. (doi:10.1021/la034783o)

Claesson, P. M., Blomberg, E., Froberg, J. C. *et al.* 1995 Protein interactions at solid surfaces. *Adv. Colloid Interface Sci.* **57**, 161–227. (doi:10.1016/0001-8686(95)00241-H)

Cramer, C. J. & Truhlar, D. G. 1999 Implicit solvation models: equilibria, structure, spectra, and dynamics. *Chem. Rev.* **99**, 2161–2220. (doi:10.1021/cr960149m)

Dee, K. C., Puleo, D. A. & Bizios, R. 2002 *An introduction to tissue–biomaterial interactions*, vol. 20. Hoboken, NJ: Wiley-Liss.

Duinhoven, S., Poort, R., Van der Voet, G., Agterof, W. G. M., Norde, W. & Lyklema, J. 1995 Driving forces for enzyme adsorption at solid–liquid interfaces. 1. The serine protease savinase. *J. Colloid Interface Sci.* **170**, 340–350. (doi:10.1006/jcis.1995.1111)

Durchschlag, H. & Zipper, P. 2001 Comparative investigations of biopolymer hydration by physicochemical and modeling techniques. *Biophys. Chem.* **93**, 141–157. (doi:10.1016/S0301-4622(01)00217-4)

Frommer, M. A. & Miller, I. R. 1968 Adsorption of DNA at the air–water interface. *J. Phys. Chem.* **72**, 2862–2866. (doi:10.1021/j100854a029)

Garcia de la Torre, J. 2001 Hydration from hydrodynamics. General considerations and applications of bead modeling to globular proteins. *Biophys. Chem.* **93**, 159–170. (doi:10.1016/S0301-4622(01)00218-6)

Graham, D. E. & Phillips, M. C. 1979 Proteins at liquid interfaces. *J. Colloid Interface Sci.* **70**, 415–426. (doi:10.1016/0021-9797(79)90049-3)

Harding, S. E. 2001 The hydration problem in solution biophysics: an introduction. *Biophys. Chem.* **93**, 87–91. (doi:10.1016/S0301-4622(01)00213-7)

Head-Gordon, T. & Hura, G. 2002 Water structure from scattering experiments and simulation. *Chem. Rev.* **102**, 2651–2670. (doi:10.1021/cr0006831)

Helfrich, J. P. 1998 Flow-mode dynamic laser light scattering technology for 21st century biomolecular characterization. *Am. Biothech. Lab.* **16**, 64–66.

Helfrich, J. P. & Jones, W. R. 1999 High-sensitivity protein aggregate characterization using flow-mode static and dynamic laser light scattering detection coupled to a size exclusion chromatograph. *Am. Biotech. Lab. Ser.* June, pp. 26–28.

Hook, F. & Kasemo, B. 2001 Variations in coupled water, viscoelastic properties, and film thickness of a Mefp-1 protein film during adsorption and cross-linking: a quartz crystal microbalance with dissipation monitoring, ellipsometry, and surface plasmon resonance study. *Anal. Chem.* **73**, 5796–5804. (doi:10.1021/ac0106501)

Hook, F., Rodahl, M., Brzezinski, P. & Kasemo, B. 1998 Energy dissipation kinetics for protein and antibody-antigen adsorption under shear oscillation on a quartz crystal microbalance. *Langmuir* **14**, 729–734. (doi:10.1021/la970815u)

Hook, F. *et al.* 2002 A comparative study of protein adsorption on titanium oxide surfaces using *in situ* ellipsometry, optical waveguide lightmode spectroscopy, and quartz crystal microbalance/dissipation. *Colloids Surf. B: Biointerfaces* **24**, 155–170. (doi:10.1016/S0927-7765(01)00236-3)

Jeon, J., Superline, R. & Raghavan, S. 1992 Quantitative analysis of adsorbed serum albumin on segmented polyurethane using FT-IR/ATR spectroscopy. *Appl. Spectrosc.* **46**, 1644–1648. (doi:10.1366/0003702924926826)

Kamyshny, A., Lagerge, S., Partyka, S., Relkin, P. & Magdassi, S. 2001 Adsorption of native and hydrophobized human IgG onto silica: isotherms, calorimetry, and biological activity. *Langmuir* **17**, 8242–8248. (doi:10.1021/la011127k)

Knezic, D. 2002 Thermodynamic properties of supersaturated protein solutions. Ph.D. thesis, Polytechnic University, New York, 242 pp.

Krishnan, A., Siedlecki, C. & Vogler, E. A. 2003 Traube-rule interpretation of protein adsorption to the liquid–vapor interface. *Langmuir* **19**, 10 342–10 352. (doi:10.1021/la035308t)

Krishnan, A., Siedlecki, C. A. & Vogler, E. A. 2004*a* Mixology of protein solutions and the Vroman effect. *Langmuir* **20**, 5071–5078. (doi:10.1021/la036218r)

Krishnan, A., Sturgeon, J., Siedlecki, C. A. & Vogleri, E. A. 2004*b* Scaled interfacial activity of proteins at the liquid–vapor interface. *J. Biomed. Mater. Res. A* **68**, 544–557. (doi:10.1002/jbm.a.20104)

Krishnan, A., Wilson, A., Sturgeon, J., Siedlecki, C. A. & Voglar, E. A. 2005*a* Liquid–vapor interfacial tension of blood plasma, serum and purified protein constituents thereof. *Biomaterials* **26**, 3445–3453. (doi:10.1016/j.biomaterials.2004.09.016)

Krishnan, A., Liu, Y.-H., Cha, P., Woodward, R., Allara, D. & Vogler, E. A. 2005*b* An evaluation of methods for contact angle measurements. *Colloids Surf. B: Biointerfaces* **43**, 95–98. (doi:10.1016/j.colsurfb.2005.04.003)

Krishnan, A., Liu, Y.-H., Cha, P., Allara, D. & Vogler, E. A. 2005*c* Scaled interfacial activity of proteins at a hydrophobic solid/aqueous-buffer interface. *J. Biomed. Mater. Res.* **75**, 445–457. (doi:10.1002/jbm.a.30444)

Lu, J. R., Su, T. J. & Penfold, J. 1999 Adsorption of serum albumins at the air/water interface. *Langmuir* **15**, 6975–6983. (doi:10.1021/la990131h)

Nuzzo, R. G. & Allara, D. L. 1983 Adsorption of bifunctional organic disulfides on gold surfaces. *J. Am. Chem. Soc.* **105**, 4481–4483. (doi:10.1021/ja00351a063)

Nuzzo, R. G., Fusco, F. A. & Allara, D. L. 1987 Spontaneously organized molecular assemblies. 3. Preparation and properties of solution adsorbed monolayers of organic disulfides on gold surfaces. *J. Am. Chem. Soc.* **109**, 2358–2368. (doi:10.1021/ja00242a020)

Nuzzo, R. G., Dubois, L. H. & Allara, D. L. 1990 Fundamental studies of microscopic wetting on organic surfaces. 1. Formation and structural characterization of a self-consistent series of polyfunctional organic monolayers. *J. Am. Chem. Soc.* **112**, 558–569. (doi:10.1021/ja00158a012)

Porter, M. D., Bright, T. B., Allara, D. L. & Chidsey, C. E. D. 1987 Spontaneously organized molecular assemblies. 4. Structural characterization of *n*-alkyl thiol monolayers on gold by optical ellipsometry, infrared spectroscopy, and electrochemistry. *J. Am. Chem. Soc.* **109**, 3559–3568. (doi:10.1021/ja00246a011)

Putnam, F. W. 1975 Alpha, beta, gamma, omega—the roster of the plasma proteins. In *The plasma proteins: structure, function, and genetic control* (ed. F. W. Putnam), vol. 1, pp. 58–131. New York: Academic Press.

Richards, F. M. 1977 Areas, volumes, packing and protein structure. *Annu. Rev. Biophys. Bioeng.* **6**, 151–176. (doi:10.1146/annurev.bb.06.060177.001055)

Rosen, M. J. 1978 *Surfactants and interfacial phenomena*, vol. 14. New York: Wiley.

Sheller, N. B., Petrash, S. & Foster, M. D. 1998 Atomic force microscopy and x-ray reflectivity studies of albumin adsorbed onto self-assembled monolayers of hexadecyltrichlorosilane. *Langmuir* **14**, 4535–4544. (doi:10.1021/la970916s)

Sigal, G. B., Mrksich, M. & Whitesides, G. M. 1997 Using surface plasmon resonance spectroscopy to measure the association of detergents with self-assembled monolayers of hexadecanethiolate on gold. *Langmuir* **13**, 2749–2755. (doi:10.1021/la961024f)

Strey, R., Vilsanen, Y., Aratono, M., Kratohvil, J. P., Yin, Q. & Friberg, S. E. 1999 On the necessity of using activities in the Gibbs equation. *J. Phys. Chem. B* **103**, 9112–9116. (doi:10.1021/jp990306w)

Vasquez, M., Nemethyt, G. & Scheraga, H. A. 1994 Conformational energy calculations on polypeptides and proteins. *Chem. Rev.* **94**, 2183–2239. (doi:10.1021/cr00032a002)

Vogler, E. A. 1992*a* Practical use of concentration-dependent contact angles as a measure of solid–liquid adsorption. I. Theoretical aspects. *Langmuir* **8**, 2005–2012. (doi:10.1021/la00044a022)

Vogler, E. A. 1992*b* Practical use of concentration-dependent contact angles as a measure of solid–liquid adsorption. II. Experimental aspects. *Langmuir* **8**, 2013–2020. (doi:10.1021/la00044a023)

Vogler, E. A. 1993 Interfacial chemistry in biomaterials science. In *Surfactant science series* (ed. J. Berg), vol. 49, pp. 184–250. New York: Dekker.

Vogler, E. A. 1998 Structure and reactivity of water at biomaterial surfaces. *Adv. Colloid Interface Sci.* **74**, 69–117. (doi:10.1016/S0001-8686(97)00040-7)

Vogler, E. A. 2001 How water wets biomaterials. In *Water in biomaterials surface science* (ed. M. Morra), pp. 269–290. New York: Wiley.

Vogler, E. A., Martin, D. A., Montgomery, D. B., Graper, J. & Sugg, H. W. 1993 A graphical method for predicting protein and surfactant adsorption properties. *Langmuir* **9**, 497–507. (doi:10.1021/la00026a023)

Wills, P. R., Comper, W. D. & Winzor, D. J. 1993 Thermodynamic non-ideality in macromolecular solutions: interpretation of viral coefficients. *Arch. Biochem. Biophys.* **300**, 206–212. (doi:10.1006/abbi.1993.1029)

Zhou, C. *et al.* 2004 Human immunoglobulin adsorption investigated by means of quartz crystal microbalance dissipation, atomic force microscopy, surface acoustic wave, and surface plasmon resonance techniques. *Langmuir* **20**, 5870–5878. (doi:10.1021/la036251d)